The Ohio State University – Department of Mechanical and Aerospace Engineering

Control Moment Gyroscope Stabilization and Maneuverability of Inherently Unstable Vehicles and Mobile Robots

By

Simon R. Kalouche
Spring 2014

Undergraduate Honors Thesis

Presented in Partial Fulfillment of the Requirements for Graduating with Honors and Distinction in Mechanical Engineering

Advisors:
Dr. Giorgio Rizzoni & Dr. Ümit Özgüner

Abstract

The control problem of stabilizing an inherently unstable body, such as the inverted pendulum, is a classic control theory problem. Traditionally, the solution to this problem has been approached through methods of dynamic stabilization where the inverted pendulum is placed on a wheeled cart that can travel with one translational degree of freedom. This cart essentially accelerates the pivot of the inverted pendulum to accelerate the pendulum to induce a rotation that counteracts the imbalance in the system. A different approach to stabilizing a static or stationary inverted pendulum makes use of the intriguing phenomena known as gyroscopic precession. Precession and the physics of gyros are governed by conservation of angular momentum. By utilizing this technology in a novel way, groundbreaking progress can be made in the field of autonomous stability of inherently unstable mobile robots and vehicles (e.g. two wheeled vehicles). Gyroscopic effects can be found today in simple devices such as a spinning top or a bicycle's wheel in motion. Gyros are also found in very complex mechanisms such as those used for satellite attitude and large ship anti-roll systems. Recent gyro studies have shown tremendous promise for providing unparalleled capabilities in stabilization and maneuverability for both on and off-road vehicle applications.

Acknowledgements

This research was performed through of the Center for Intelligent Transportations Research (CITR) Laboratory located at The Ohio State University's Center for Automotive Research (CAR). I would like to recognize Dr. Umit Ozguner, Dr. Codrin-Gruie Cantemir, Dr. Keith Redmill, Harun Yetkin, Michael Vernier, Dan Kestner, and Greg Colvin for their constructive feedback, useful knowledge, and time dedicated to ensuring the success of this project and thesis. I would also like to thank The Ohio State University for making readily accessible countless resources. Finally, I would like to thank the Air Force Research Lab for the inspiration and funding for this research.

Contents

List of Figures

List of Tables

1 Introduction

1.1 Motivation

In 2011, the Air Force Research Lab (AFRL) of Dayton, OH, operating through Wright-Patterson Air Force Base developed a program known as the Special Ops Transport Challenge. This challenge was created to fill a current void in Special Operations type missions where existing solutions were not sufficient—a consequence of the evolving tactics of warfare. The AFRL challenge desired the research, design, and fabrication of a semi-autonomous, off-road vehicle capable of transporting two soldiers and their payload (estimated at 700 lbs) over very rugged and mountainous terrains.

The vehicle was to meet a list of several strict operating objectives and design requirements. The AFRL needed a vehicle, ultimately geared towards Special Operations type missions such as insertion or recovery of troops, that could operate quickly and in a stealth manner as to not be detected easily visually or audibly. The vehicle is expected to have the capability to travel over an approximate total distance of 60 kilometers and must operate in a fashion that exceeds the capabilities of all current and conventional off-road vehicles in terms of traversing/scaling obstacles (i.e. large rocks, narrow paths, small cliffs, etc.). The vehicle must permit for storage and deployment via CV-22 Osprey Helicopter whose storage container is dimensioned at 5 x 5 x 18 feet. The vehicle must also be operable within four hours of removal from storage (i.e. minimal assembly time desired). It is expected that the vehicle be operable during the day, night, and inclement weather, or any conditions the CV-22 is capable of flying in. The AFRL requires a certain level of autonomy in the vehicle so that the personnel operating the vehicle can ideally be trained in one day or less. AFRL and OSHA safety standards must be met or exceeded in the vehicle's design [1].

With regards to the AFRL challenge requirements and strict size constraints, traditional off-road vehicles and their limitations were analyzed. Current off-road vehicles include: Humvees, jeeps, dune buggies, pick-up trucks, all-terrain-vehicles (ATV's), dirt bikes etc. Although each of these platforms is advantageous in its designated area of performance, when each of their characteristics was analyzed with respect to the AFRL's requirements all of these vehicles had major insufficiencies. For example, Humvees, like other traditional four-wheeled vehicles, are limited by overall size and obstacle overcoming capabilities. The Humvee exceeds the available storage container size of a CV-22 Osprey, and can only surmount a vertical obstacle with a height equal to the radius of the vehicles tires, which varies by vehicle but is on the order of 2 to 3 feet maximum. Dune buggies have a similar issue with transcending obstacles as their natural and aggressive stance is designed to keep the chassis low to the ground. ATVs, on the contrary, are very agile on rugged terrains, however they have passenger and payload limitations. It is not feasible for two soldiers and all of their gear to travel 30-60 km over very rugged terrains on an ATV safely. Similarly dirt bikes, although very capable when it comes to traveling on uneven terrain or surmounting obstacles, have passenger limitations and require heavy training to become sufficient at riding over highly rugged terrains. Therefore, it was determined that all existing off-road vehicle platforms were not fully capable of meeting the rigorous requirements set forth by the AFRL. This determination eliminated the possibility of modifying a traditional off-road vehicle to meet the required specifications, posing the opportunity to develop a novel vehicle platform.

Thus, alternative solutions were explored. Consideration of flying vehicles were quickly deemed unpractical due to the large energy requirements, the magnitude of required training, and the inherently loud and non-stealth operating mode of most basic air vehicles. Hovering vehicles were considered as well, but due to their large energy

requirements and inability to travel over very rugged or heavily inclined terrains this option was also determined to be inadequate. The third option that was considered was a gyroscopically stabilized vehicle. This option allowed for a very thin vehicle whose gyros could, theoretically, balance and maneuver the vehicle about all 3 of the vehicles axes. This un-paralleled capability offers numerous advantages over traditional off-road vehicles in terms of autonomous stabilization and scaling obstacles. The basic structure of this vehicle concept consists of two large (greater than 5 ft. diameter) wheels oriented in tandem, similar to a bicycle, where each soldier rides inside of one of the large monowheels. The vehicle will be stabilized, balanced, and maneuvered via a set of optimized Control Moment Gyroscopes (CMGs). A general concept design rendering of the vehicle can be seen in Figure 1.

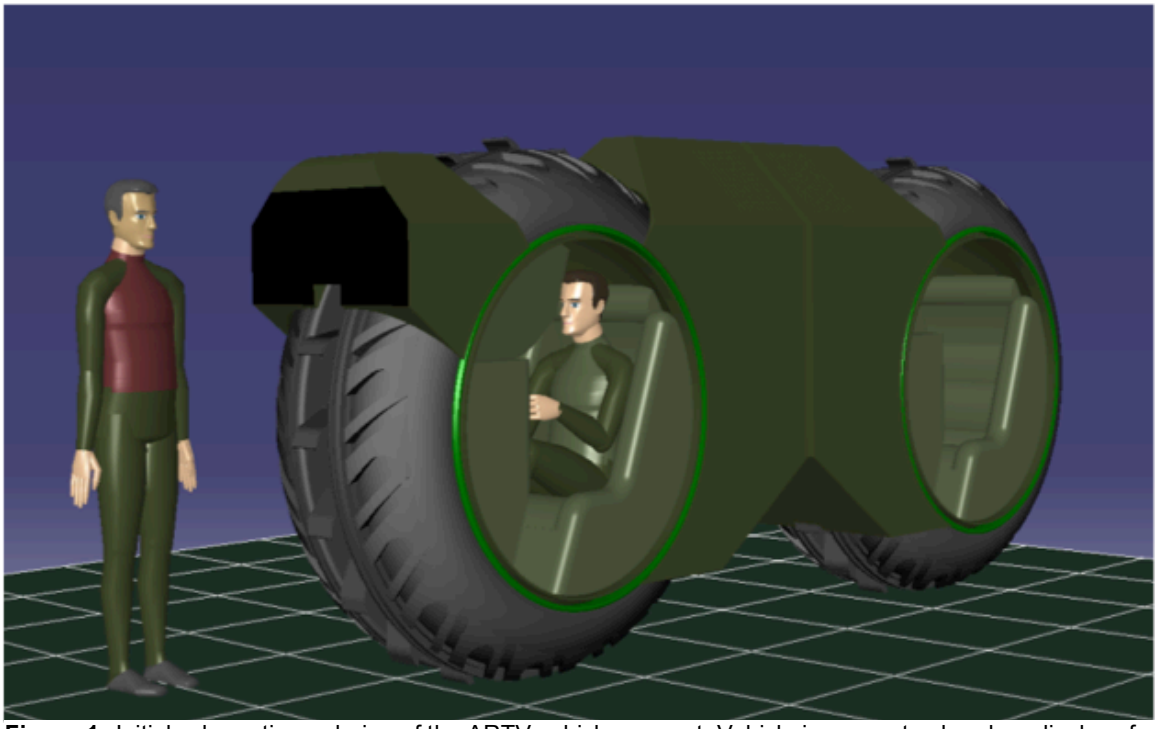

Figure 1: Initial schematic rendering of the ARTV vehicle concept. Vehicle incorporates head-up displays for front and rear vision among many other features.

1.2 Background

By approaching maneuverability and stabilization of an off-road vehicle in non-traditional methods, the maneuverability of the vehicle can be significantly enhanced. The Ohio State Agile Rugged Terrain Vehicle (OSU ARTV) team is developing a vehicle that will have enhanced maneuverability unseen in traditional off-road vehicles. To achieve this level of maneuverability, a multi-axis gimbal Control Moment Gyroscope (CMG) stabilization system is used, which can allow the vehicle to surmount or pass unusually difficult obstacles within a given terrain. The focus of this thesis is to apply the theory behind CMG stabilization to an experimental bicycle test bed to validate the core stabilization and maneuverability concepts proposed by the future OSU ARTV vehicle. The derivation of the static and dynamic equations of motion and the experimental results of this pre-prototype bicycle platform will be used to design the mechanical systems and control algorithm of the AFRL vehicle.

There are, theoretically, two methods by which a two-wheeled vehicle oriented in tandem can be stabilized: dynamic stabilization and CMG (control moment gyroscope) stabilization. Dynamic stabilization utilizes high feedback tactical steering techniques to generate or trigger a lean in the vehicle in the intended direction for counter acting the body's imbalance. Conversely, CMG control employs the conservation of angular momentum of a high RPM flywheel to generate an amplified reaction torque about the

Figure 2: Brennan's Monorail [2]

Figure 3: Shilovsky's Gyrocar [3]

axis that will balance the vehicle. Of these two, CMG offers greater advantages on static vehicles. Although not very intuitive, CMG stabilization has been demonstrated since the beginning of the 20th century. Two notable vehicles that apply this technology on inherently unstable vehicles are Shilovsky's Gyrocar and Brennan's Gyroscopic Monorail shown in Figure 3 and Figure 2 [2][3]. However, because of limited electric motor technology, motors at the time of production for these vehicles (1906) could only reach speeds of 3000-4000 rpm for spinning the flywheel, and were very expensive custom made motors [4]. Also, at the time, control techniques for these gyro stabilization systems were purely mechanical thus lacking sensor feedback to ensure adequate balancing over even small disturbances [2]. Therefore, it had been more practical to continue developing and mass-producing four wheeled, inherently stable, vehicles instead of pursuing CMG stabilization [2]. However, today much progress has been made in electric motor technology as compared to a near century ago. Today, much higher performing motors exceeding 20,000 revolutions per minute are mass-produced and can be bought for just a few hundred dollars [5]. Currently, a recent start-up company based out of San-Francisco, CA, called Lit Motors, is using a set of 2 counter rotating single axis gimbal gyro's to stabilize and autonomously balance an enclosed motorcycle [6]. This completely electric vehicle shown in Figure 4, in the making for

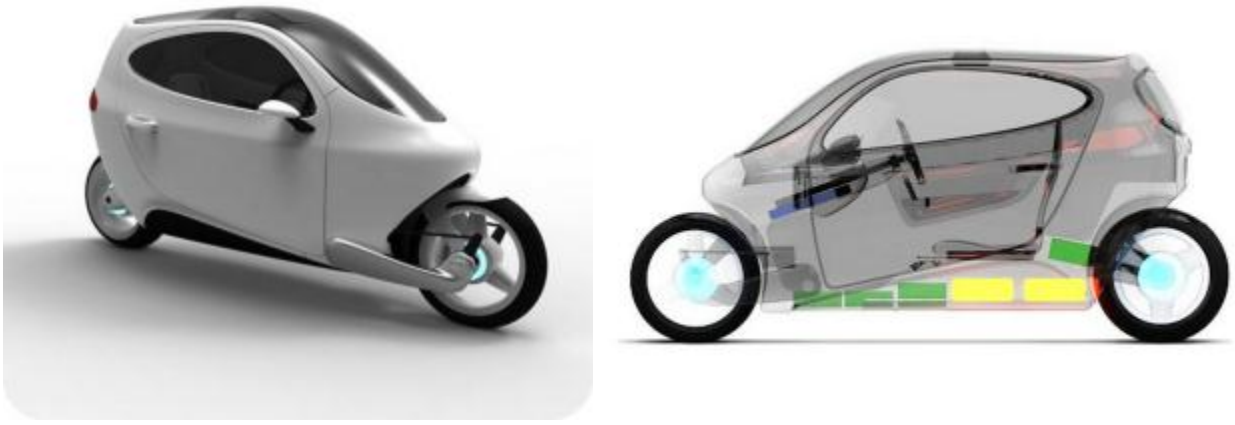

Figure 4: Lit Motor's self-balancing prototype vehicle rendering. Vehicle uses two counter-rotating gyros (shown in yellow) to achieve stability.

several years now, has proven through prototype success the capability to stabilize and self-balance a street-ready vehicle that can transport up to two people [6].

Gyroscopic applications are either passive or active systems. Passive gyroscopic systems require no gimballing actuators and imply the use of a spinning flywheel to oppose change in angular momentum (rotation) over the input of a disturbance. This method of balancing has been used in large ships or vessels and utilizes a large spinning flywheel's angular momentum to avoid rolling or tilting from applied external forces from waves. This passive system means that the flywheels large moment of inertia and angular momentum make it more difficult for the boat to tilt because the flywheel opposes any change in orientation or angular rotation; therefore, when rigidly fixed to the ship without a gimbal, the ship also opposes angular rotation (i.e. tilting to one side or the other). The same phenomenon is displayed in a bicycle moving straight. It can be noted that the faster the bicycle moves the easier it is to balance on the bicycle [7]. This is because the wheels of the bicycle act as passive flywheels. When the angular momentum of the wheels increases with the increase in translational speed of the bicycle (proportional to the angular velocity of the wheels), the bicycle also experiences an increase in its opposition to angular rotation or tilting, making it easier to remain upright and balanced on a faster moving bicycle than on a slow or stationary bicycle [7].

The second method used in gyroscopic applications is an active system. An active system implies the use of one or more gimballing mechanisms and actuators that can rotate a spinning flywheel about an axis perpendicular to its spin axis to induce a precession or reactive torque about an axis perpendicular to both the gimbal and spin axes. This reactive torque can be useful for a variety of purposes for trivial and non-trivial applications. An example of an active gyroscopic system can be seen in use on orbiting space satellites. Due to the lack of gravity and air resistance in space it is very

difficult to accurately orient or rotate a satellite in the correct direction through the use of conventional rotational actuating and propulsion techniques. Therefore, several separate single-axis gimballing gyros or a multi-axis gimbal gyro can be used to rotate the satellite to its desired attitude relative to the body being orbited [8]. Because single-axis gyros are simpler, more efficient, and experience fewer singularities, most active gyroscopic systems employ multiple single-axis gimballing flywheels to achieve the same 3-degree of freedom control effect as a single multi-axis gimballing system [8].

1.3 Focus of Research

Given that gyroscopic stabilization technology has been previously utilized and considering the benefits it offers in terms of fulfilling the AFRL vehicle requirements, developing this concept showed promise in revolutionizing the capabilities of off-road vehicles. The focus of this research thesis is dedicated to demonstrating a proof of concept for this gyro stabilization technology and validating its ability to autonomously balance an unmanned static bicycle. Iterations of this balancing proof of concept have been demonstrated on a predecessor inverted pendulum test platform, but this study aims to demonstrate balancing and maneuverability techniques on a platform that more closely resembles the geometry and degrees of freedom (DOF) of the actual prototype vehicle: a bicycle.

This thesis will also look into the design for a gyro system capable of inducing and temporarily maintaining a ‘wheelie’ type motion on a bicycle. This type of maneuverability motion is what makes the ARTV’s prototype vehicle more capable than any other currently existing vehicles.

1.4 Thesis Outline

Chapter 2 of this thesis will elaborate on the theory behind how control momentum gyroscope technology works and how a bicycle can be stabilized using an actuated single-axis gimbal CMG configured system. Chapter 3 will focus on the design optimization and theoretical control of a CMG system capable of inducing advanced maneuvers on a bicycle. The calculations and methodology used to design the hardware and components for the bicycle pre-prototype platform will be presented. Chapters 3 and 4 will explore and quantify the results of Simulink model simulations as well as physical experimental tests done on the bicycle pre-prototype for both balancing and maneuverability applications.

2 Control Momentum Gyroscope Theory

2.1 Concept Considerations

When comparing CMG stabilization to the more traditional approaches taken to stabilize inherently unstable robots and vehicles the advantages and disadvantages must be thoroughly analyzed for each specific application. In the case of developing a stable and very mobile vehicle the advantages offered by a CMG significantly outweigh the challenges or disadvantages associated with utilizing this form of stabilization. The following sections elaborate further on why CMG technology is auspicious for off-road, highly maneuverable vehicles.

2.1.1 Advantages

Using non-traditional CMG methods to stabilize an inherently unstable body offers numerous and promising advantages with respect to an off-road vehicle application. A vehicle equipped with a CMG system can theoretically exceed performance capabilities of all existing vehicles. A CMG system can not only provide

stabilization torques for inherently unstable vehicles and robots (e.g. a two wheel in tandem vehicle, legged robot, etc.) but it can also induce advanced and very controllable maneuvers on the vehicle such as lifting up from the ground its front or rear tire. This wheelie type motion will allow the vehicle to climb or surmount very large rocks or changes in level of terrain on the order of 4 to 5 feet as opposed to the 2-3 foot limit of Humvees. Using a CMG rather than mechanisms is simpler and reduces the size of the vehicle.

CMG systems are also power efficient because of the mechanical advantage offered by a flywheel's torque amplification. Driving energy consumption will also be lowered when considering the reduction of weight accomplished by eliminating 2 wheels and portions of the chassis from the vehicle. Energy consumption to power the flywheel is dependent on the flywheel's radius, mass, and operating speed; however, the majority of the flywheel's power consumption occurs in the initial acceleration of the flywheel. Once the flywheel is up to speed additional energy is only needed to account for losses due to bearing friction and air drag. Further energy savings can be accomplished by using high performance bearings and imbedding the flywheel into a vacuum chamber to eliminate losses due to air drag. These characteristics give CMG stabilized vehicles the potential to be very energy efficient—an ideal property for long range Special Ops missions as well as for civilian city vehicles.

2.1.1 **Disadvantages**

Although the advantages of using a CMG system to stabilize a vehicle seem to significantly outweigh the disadvantages, the challenges of utilizing a CMG system must be considered. A vehicle equipped with a multi-axis gimbal CMG or even a single-gimbal CMG has rather complex dynamics and the systems are dependent on and responsive to a large amount of design and control parameters. This means that control of the CMG

systems to produce desired vehicle behavior is very complex and dependent on many variables. Some of these variables must be determined via accurate sensor feedback while others must be calculated instantaneously to achieve desired vehicle motion. Therefore the only significant disadvantage of CMG stabilization systems for vehicles is the added complexity of control and analyzing system response associated with multi-body dynamics required to drive as opposed to a four wheeled vehicle that is inherently stable and therefore requires little to no control for stabilization [2]. Further complexities arise in modeling the dynamic behavior of a two-wheeled vehicle in turning where a desired lean would need to be induced and maintained by the flywheel. This thesis focuses on the stabilization control of a static, non-moving, bicycle.

2.2 Angular Momentum

The fundamental principle that describes the behavior and response of a spinning flywheel is the conservation of angular momentum. This law describes the behavior of a spinning flywheel's motion in response to an applied external force or torque as well as the flywheel's motion when external forces and torques sum to zero. For the focus of this thesis the geometry of interest for the gyro will always be modeled as solid disk whose thickness is close to one fourth the diameter.

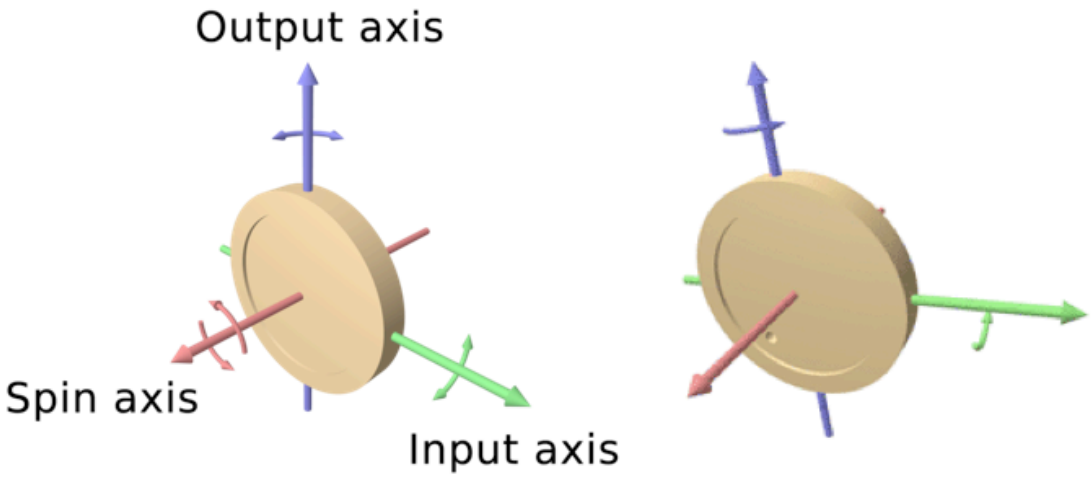

Figure 5: Rotating flywheel with axes labeled. Input axis (green) is the flywheels gimbal axis and the reactive torque occurs about the output (purple) axis (left). Flywheel, unconstrained, motion shown with corresponding gimbal and precession rotation shown (right) (source: Wikipedia).

According to Newton's 1st law of motion, an object in motion will stay in motion unless acted on by an external force. This statement holds true for rotating objects as well. Therefore, a spinning flywheel (constant spin rate) with no applied external forces or torques will continue to spin about its spin axis, in its current orientation, with no other rotational or translational motion relative to a stationary frame of reference. However, a spinning flywheel with summation of external forces or torques (about an axis other than its spin axis) not equal to zero exhibits an interesting phenomenon called precession [9]. Because angular momentum is a vector both the direction and magnitude are important in quantifying this property of the flywheel. The direction of the angular momentum is shown by the red arrow in Figure 5. Now consider, the flywheel spinning at a constant spin rate, ω, with a constant angular momentum (L) calculated by equation 1.

$$I_{disk} = \frac{1}{2}mr^2 \tag{1}$$

$$L = I\omega = \left(\frac{1}{2}mr^2\right)\omega$$

To observe the precession effect caused by a rate of change of angular momentum, the flywheel must rotate about an axis perpendicular to its spin axis. This rotation about a perpendicular 'gimbal' axis (e.g. the green axis in Figure 5) must be generated via an external torque. Once this rotation occurs, a simultaneous rotation will occur about the other orthogonal 'precession' axis (the purple axis in this example). It is important to note that precession is caused by a rate of change in the flywheel's angular momentum; therefore, precession only occurs when the flywheel is being gimbaled (i.e. $|\dot{\alpha}| > 0$ where $\dot{\alpha}$ is the flywheel's gimbal rate. This simultaneous resultant rotation about the purple axis is called reactive precession and is a direct result of the flywheel conserving its angular momentum. Precession, however, is extremely useful for the mechanical advantage it offers, known as torque amplification. The torque generated

from gimballing the spinning flywheel about an axis orthogonal to its spin axis is dependent on, and a function of, the angular velocity or rate of gimbal (assuming constant flywheel geometry and spin angular velocity) [9].

The direction of rotation of this precession is dependent on the direction of angular momentum as well as the direction of the externally applied torque about the green or gimbal input axis. The resulting rotation (i.e. precession) would be identically flipped had the external torque been applied to the purple axis, or the external torque applied in the opposite direction about the green gimbal axis.

To fully understand how and why precession occurs an example scenario will be explained. Given a spinning flywheel, Figure 6 with constant spin rate (rotating CCW about the x-axis) and an angular momentum (green arrow) pointing to the negative 'x' direction (180°) initially, a series of conditions must occur for the angular momentum to be reoriented to point to an angle larger than 180° with no component in the z-axis (angular momentum remains in x-y plane only). Shown in Figure 6 is the schematic of the initial and final positions of the flywheel. The change in flywheel orientation (angular momentum) shown in Figure 6 corresponds to the flywheel rotating purely about one axis: the gimbal or z-axis. This motion of purely rotating about the gimbal axis without simultaneous rotation about the precession axis is not natural, meaning an external torque must be applied on the system to counteract the reactive torque generated by precession. By the summation of angular momentum vectors,

$$\overrightarrow{L_o} + \overrightarrow{L_\iota} = \overrightarrow{L_f}$$

where, $\overrightarrow{L_o}$ is the initial angular momentum of the flywheel, $\overrightarrow{L_\iota}$ is the intermediate change in angular momentum, and $\overrightarrow{L_f}$ is the final angular momentum. By Newton's 2nd law, for the flywheel to rotate about the z-axis without precessing or rotating about the y-axis, an external torque must be applied about an axis coincident with the intermediate vector $\overrightarrow{L_\iota}$

in the direction specified by the right hand rule (where thumb points in the direction of $\overrightarrow{L_i}$), which in this scenario would be counter clockwise (CCW). This means that, had there been no external torque applied, the flywheel would have naturally precessed about the y-axis in the clockwise direction, which would have resulted in a component of the angular momentum coming out of the x-y plane. An important behavior of this conservation of angular momentum concept to consider is the precession motion relative to a fixed frame (or coordinate system) as opposed to a frame that rotates with the gimballing flywheel [10]. Observing precession from a fixed frame of reference shows that at the instantaneous moment when the flywheel begins to gimbal, the precession occurs simultaneously about the orthogonal precession axis, which at this initial instant is exactly coincident in both the fixed and freely rotating frames of reference. However, as the flywheel continues to gimbal, the precession continues to occur about the flywheel's own freely rotating precession axis (rotating coordinate system) which is no longer coincident with the fixed frame of reference's (or the flywheel's original position) precession axis [11] [12]. So, relative to the fixed frame, which is coincident with the flywheels original position prior to any gimballing, the rotation due to precession (after the first instant) is composed of two components. One component is about the fixed

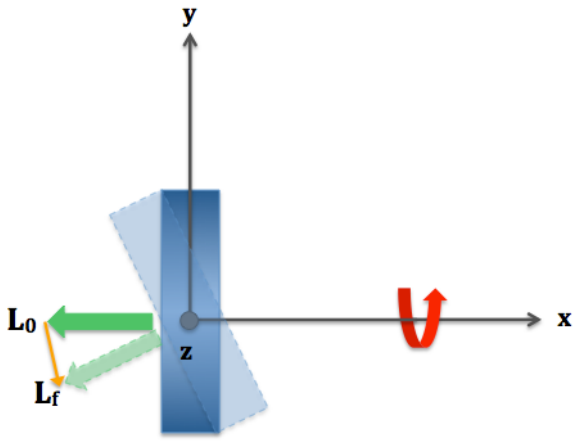

Figure 6: Schematic of flywheel angular momentum vector addition.

frame's precession axis, and the second component is about the fixed frame's spin axis. Relative to the flywheel's rotating frame of reference, there is always only one component of precession, which is always about the rotating frame's precession axis. Therefore, after the flywheel has gimbaled more than 45 degrees, the component of the reactive precession about the fixed frame's precession axis will be less than the component of reactive precession about the fixed frame's spin axis. At the gimbal position of exactly 45 degrees the two components (relative to the fixed frame) will be exactly equal; when the gimbal angle is less than 45 degrees the component about the fixed frame's precession axis will be greater. This effect will limit the effective gimballing range of the CMG to be within $\pm 45°$ which is taken into account in the design and control of the CMG system.

2.3 Governing Equations of Motion

Using a Lagrangian approach two coupled ordinary differential equations (ODE) were derived to explain the governing motion of a gyro on a hinge system given a set of initial conditions. The gyro on a hinge, mimicking the three degree of freedom mobility of

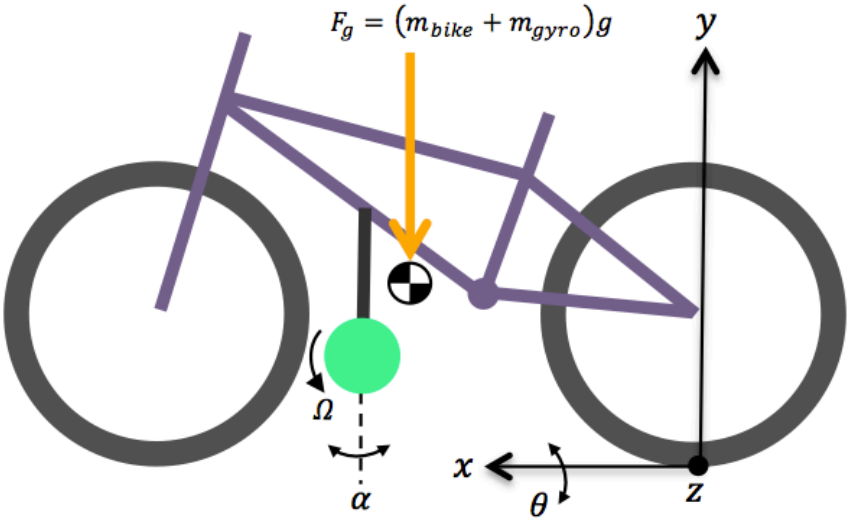

Figure 7: Bicycle modeled with three degrees of freedom $\boldsymbol{\theta}, \boldsymbol{\alpha}, \boldsymbol{\Omega}$ and the center of mass location shown.

the bicycle, is modeled as an inverted pendulum, defined as having the center of mass above the pivoting joint, and constrained to rotation about just the x-axis. The gyro is modeled as a thin disk of constant width. The system described above and shown in Figure 7 has three rotational degrees of freedom: θ, α, and Ω. Theta (θ) is the bicycle's perturbation angle from the vertical (rotation about the x-axis), where $\theta = 0°$ is the bicycle's unstable equilibrium. Alpha (α) is the angular position of the flywheel's gimbal and Ω is the rotational degree of freedom about the flywheel's spin axis. The initial steps of the derivation of the governing equations of motion are shown below. An explicit derivation is provided in Appendix A.

$$L(\theta, \alpha) = \mathrm{T} - \mathrm{V} \tag{2}$$

where,

$$\mathrm{T} = \text{kinetic} = \frac{1}{2} I_{bike} \dot{\theta}^2 + \frac{1}{2} \int_{GYRO} dm \left(\dot{\vec{x}}_{GYRO}\right)^2$$

$$V = \text{gravitational potential} = \left((M_{bike})(g)\left(h_{bike_{COM}}\right) + M_{gyro} * R \right) cos\, \theta = V_o$$

The Euler-Lagrange Equations follow as,

$$\frac{\partial \mathrm{L}}{\partial \theta} = \frac{d}{dt}\left(\frac{\partial \mathrm{L}}{\partial \dot{\theta}}\right)$$

$$\frac{\partial \mathrm{L}}{\partial \alpha} = \frac{d}{dt}\left(\frac{\partial \mathrm{L}}{\partial \dot{\alpha}}\right)$$

After the full derivation of the total energy within the gyro inverted pendulum system, a set of two, second order, non-linear, Ordinary Differential Equations (ODE's) of motion were found, where the list of used variable and parameters can be found in Table 1.

$$\left(I_{bike} + m_{fly}R^2 + \frac{1}{4}m_{fly}r_g^2(1+\sin^2\alpha)\right)\ddot{\theta} + \frac{1}{2}m_{fly}(r_g^2)(\dot{\alpha})\dot{\theta}\sin\alpha\cos\alpha \ldots$$

$$\ldots - \frac{1}{2}m_{fly}(r_g^2)(\Omega)\,\frac{d(\sin\alpha)}{dt} - \mathrm{V}_o\sin\theta = 0 \qquad (3)$$

$$0 = \ddot{\alpha} - \sin\alpha\cos\alpha\,\dot{\theta} + 2\Omega\dot{\theta}\cos\alpha \qquad (4)$$

where the Initial conditions are given by,

$$\theta(0) = \theta_0$$

$$\alpha(0) = \alpha_0$$

$$\dot{\theta}(0) = \dot{\alpha}_0$$

$$\dot{\alpha} = 0$$

Table 1: List of system variables and parameters used in the Lagrangian derivation

Variable / Parameter	Symbol	Unit
Gimbal angle	α	$[rad]$
Bicycle tilt angle (from vertical)	θ	$[rad]$
Length of arm from hinge to flywheel center	R	$[m]$
Rotational spin speed of flywheel	Ω	$[rad/s]$
Flywheel mass	$m_{fly} = \mu * \pi * r_g^2$	$[kg]$
Flywheel width	w	$[m]$
Flywheel material density	ρ	$[kg/m^3]$
Gyro mass	$m_{gyro} \approx 1.667 m_{fly}$	$[kg]$
Flywheel Radius	r_g	$[m]$
Mass of bicycle	m_{bike}	$[kg]$
Distance from ground to bicycle COG	h_{bike}	$[m]$
Acceleration due to gravity	g	$[m/s^2]$
Bicycle's moment of inertia about z axis	I_{bike}	$[kg/m^2]$
Angular Momentum of spinning flywheel	L_g	$\frac{kg\times rad}{m^2\times s}$

Equations 3 and 4 describe the motion of the 3 DOF system in response to a perturbation from the stable position of the inverted pendulum (i.e. when θ≠0).

The derived governing differential equations of motion are highly non-linear; therefore, modeling and simulating this system would be complicated. However, three assumptions considerably simplify and reduce the governing equations to a system of linear equations that can still accurately model the system's response. The first assumption is that the angular velocity about the gimbal axis ($\dot{\alpha}$) will only be an input parameter, thus it will not be affected by the dynamics of the system. This statement assumes that the gimballing actuator has enough torque to counteract any precession that may occur due to leaning in the bicycle and that the angular velocity, $\dot{\propto}$, is an input determined by the controller depending on how much reactive torque is needed to stabilize the unstable body. This assumption simplifies the system by decoupling the gimbal angle, α, from the bicycles angular position θ, forcing any rotation about the gimbal axis to always be an independent input to the system rather than an output dependent on the system's motion. Therefore α and its derivatives are all inputs to the system where the bicycle's angular velocity, $\dot{\theta}$, is dependent on the gimbal velocity $\dot{\alpha}$, but the gimbal velocity is not dependent on the bicycles motion. The second simplifying assumption made is that the angular velocity about the spin axis (Ω) will also be an input and held at a constant rate because varying this parameter offers no advantage in stabilization but adds complexity to the system controls. The third assumption is that the passive effects of the gyro are small in comparison to the reactive torque produced and can therefore be neglected in the system dynamics.

Thus, considering the simplifying assumptions, the function that describes the inverted pendulum's motion is dependent on 3 varying parameters: the inverted pendulum's angular position θ with respect to the gravity vector, the angular acceleration of the inverted pendulum $\ddot{\theta}$, and the angular velocity $\dot{\propto}$ about the gimbal axis. All other parameters remain constant and will be addressed in the following sections. Knowing

the first two parameters of the system at all times (by utilizing IMUs, gyroscopes, and accelerometers with closed loop control), the 3rd variable, gimbal angular velocity ($\dot{\alpha}$), can be calculated by the controller to induce a torque capable of stabilizing the system.

To model and simulate the response of the bicycle configured with a single axis gimbal gyro a simplified equation of motion was derived using the assumptions stated above. The bicycle (without the gyro) can be modeled as a one degree of freedom (DOF) inverted pendulum, where rotation is constrained to only about the x-axis. It is assumed that the friction between the tires and the ground will prevent the bicycle from rotating about the y-axis and its assumed that the small single gyro used for stabilization is unable to produce enough torque to generate rotation about the z-axis which would lift either the front or back tire off the ground. For these reasons the bicycle can be modeled as a single DOF system. Thus the governing equation of motion for the bicycle (with no gyro) is

$$\ddot{\theta} - \frac{g}{l}\sin\theta = 0$$

$$\ddot{\theta} = \frac{g}{l}\sin\theta \tag{5}$$

Because $\ddot{\theta}$ is inversely proportional to moment of inertia (I), the further away the center of mass is from the pivot, the slower the angular acceleration ($\ddot{\theta}$) will be. Using an accelerometer and Inertial Measuring Unit (IMU) feedback to sense θ and $\ddot{\theta}$ is equivalent theoretically to the following equation of motion for a 1-DOF inverted pendulum without a gyro. The Simulink model created will use closed loop feedback, which the sensors will physically approximate.

$$\tau = I\ddot{\theta}$$

$$m\ g\ l\sin\theta = I\ddot{\theta}$$

$$m\ g\ l\sin\theta = m\ R^2\ddot{\theta}$$

$$\frac{gl}{R^2}\sin\theta = \ddot{\theta}$$

$$\therefore \quad \ddot{\theta} = \frac{g}{l}\sin\theta = \frac{g}{h_{bike}}\sin\theta \tag{6}$$

[for a passive system]

2.3.1 **Flywheel Properties**

The concept of stabilizing an inherently unstable body (i.e. inverted pendulum, bicycle, mobile legged robots, etc.) utilizes the mechanical advantages offered by a high rpm flywheel's conservation of angular momentum. The angular momentum of a flywheel is a function of several parameters. Many of these parameters will be held constant in mathematical calculations and simulations because they are either physical properties of the flywheel (i.e. mass, radius, density, etc.) or because varying that parameter would offer no advantage. Therefore, control would be simpler by holding these parameters constant.

2.3.2 **Torque Amplification**

The main mechanical advantage of CMG or gyroscopic technology is a flywheel's ability to conserve its angular momentum in a way that when given an input torque about the flywheel's gimbal axis, a simultaneous output torque about the precession axis is generated, whose magnitude can be amplified by orders of magnitude. The function describing this torque amplification is derived in the following manner where the integral is taken over the angle β for the full circumference of the flywheel.

$$\tau_{gyro} = \int_0^{2\pi} \frac{2m_{fly}}{2\pi}(\Omega)\dot{\alpha}r_g\,(\sin\beta)(\mathrm{r_g}\sin\beta)\,d\beta$$

$$\tau_{gyro} = \frac{m_{fly}}{\pi}(\Omega)(\dot{\alpha})r_g^2\int_0^{2\pi}\sin^2\beta\;\;d\beta$$

$$\tau_{gyro} = \Omega\dot{\alpha}m_{fly}r_g^2 = \dot{\alpha}L_g \tag{7}$$

Therefore, the reaction torque produced by gimballing a flywheel (gyro) is a function of 4 parameters: the flywheel's mass, radius, spin rate Ω, and gimbal rate gimbal $\dot{\propto}$.

2.4 Single-Axis Gimbal CMG Systems

By focusing on the single-axis gimbal CMG system that will be designed for the bicycle as a simple function with an input, output, and constant parameters, the system can be simplified. Given a single-axis gimbal system with 360 degrees of rotation a reactive torque can theoretically be produced about 2 principle axes of the stationary frame of reference. This is due to the reactive torque being produced about an axis orthogonal to both the spin axis and the gimbal axis. When the flywheel rotates (gimbals) 90° from it's original orientation its reactive torque becomes about the stationary axis that was originally coincident with the flywheels spin axis. Because of this property, one flywheel can be used to generate both a balancing torque and a wheelie inducing torque dependent on the flywheel's initial orientation.

By adjusting the inputs and constants of the system via control and design respectively, the output of the system can be optimized to deliver the maximum and most appropriate torques for balancing the bicycle.

The inputs of this gyro function are the gimbal's angular velocity about gimbal axis (Figure 5 shown in green). By sensing the angular position and acceleration of the bicycle, a dynamic control algorithm can be developed using the system's governing equations of motion. Using the simplified dynamic equations of motion that will be derived, the controller can then determine what the appropriate gimbal velocity and gimbal time duration should be to generate the required torque to stabilize the bicycle within the gyro's range of operation (i.e. less than ±90°, and ideally less than ±45°).

As stated previously, the constants in this system function are determined by the mechanical design of the system. The flywheel's properties were optimized by graphing

the output torque produced by a flywheel with a given gimbal rate and varying radii and weight. The amount of required torque to stabilize the bicycle at varying degrees of tilt from the vertical was also plotted. Because the required reactive torque is dependent on the weight of the bicycle with the gyro system mounted, as the weight and size of the flywheel increase, so does the required torque. Therefore, a simultaneous optimization of both parameters was needed to design the most effective flywheel. This design process is elaborated in section 3.1. However, once the flywheel was designed its properties (mass, and radii) in the governing equations remained constant values. In addition to the flywheel's physical characteristics, the spin rate was also held constant at a high rate (upwards of 5000 rpm). If this parameter were varied, control would become more complex in addition to the added complexity of adding brakes and a more powerful motor to rapidly slow down or accelerate the flywheel.

The output of the system is the reactive torque created gimballing the high rpm flywheel. For a given flywheel gimbal rate $\dot{\alpha}$, a very controllable output torque can be produced about the precession axis, which is orthogonal to the spin and gimbal axes. The gyro will be designed and oriented on the bicycle so that its precession axis coincides with the pivot axis of the bicycle (x-axis as shown) to balance an unstable bicycle.

2.5 Balancing and Stabilization Algorithm

In the design of an adequate single-axis CMG used to stabilize an unmanned static or dynamic bicycle 2 parameters must be constrained. The first system constraint is orienting the flywheel so that its reactive torque is about an axis that will stabilize the bicycle. Therefore, if the flywheel is oriented as shown in Figure 12 the gyro must gimbal about only the y-axis. This will ensure that the reactive torque generated by gimballing the flywheel will be about either the x-axis which is the axis the bicycle rotates about

when falling or about the z-axis which when rotated about will generate a wheelie. Depending on the initial orientation of the flywheel, if the angular momentum points in the direction of $\pm$ z-axis then the reactive torque will be about an axis orthogonal to both the spin axis (z-axis) and the gimbal axis (y-axis). This means that the reactive torque will be applied about the x-axis, which is the correct orientation for stabilizing the bicycle if it is leaning or falling to either side. If the flywheel is initially oriented so that is angular momentum points in the direction of $\pm$ x-axis then the reactive torque will be applied about the axis orthogonal to the spin (x) and gimbal (y) axis which in this orientation means the reactive torque is applied about the z-axis. The latter orientation is used in situations where inducing advanced maneuvers such as wheelies is desired. Therefore, by constraining the flywheel to rotation about only the y-axis with angular momentum pointing in the direction of $\pm$ z-axis, the flywheel is ideally oriented to stabilize the bicycle. The 2nd constraint, which is inherent to fixing the flywheel to only rotate about the y-axis, is to fix the gyro from rotating about the x-axis. Because the flywheel, when unconstrained, will precess upon the application of an external torque provided by a servomotor the method to convert the motion of precession into a reactive torque is to not allow the flywheel to precess. By fixing the flywheel from rotating about the x-axis it will not be able to precess and therefore its motion will be translated into a torque that will then be transferred to the frame of the bike and act about the bike's balancing axis.

Once the gyros gimbal is constrained to one rotational degree of freedom (about the y-axis) the control algorithm can be developed. The control for the bicycle is dependent on several factors, which include the bicycle's current angular position relative to the semi-stable upright position, the bicycle's first and second angular position derivatives (i.e. angular velocity and acceleration), and the direction the bicycle is falling or leaning towards. Therefore for adequate stabilization, closed loop sensor feedback is crucial and a variety of sensors will need to be utilized to achieve accurate

instantaneous bicycle position feedback. A more elaborate description of the sensors used can be found in section 3.1.3. Using feedback from accelerometers or an IMU it can be determined if the bicycle is losing stability and falling either to its right or left depending on the acceleration and orientation signals processed by the sensors. With this instantaneous knowledge the gyro can gimbal up to $\pm 90°$ where the optimal range is described earlier in section 2.2 as being $\pm 45°$ to ensure that the majority component of reaction torque is acting about the desired axis to stabilize the bike and not about another axis. If the bicycle (as shown in Figure 12) is unbalanced, leaning in the clockwise (CW) direction, assuming the flywheel's angular momentum is pointing to the negative z-axis (meaning it is spinning clockwise looking at it from the right side view), then the flywheel must be gimbaled counter clockwise (CCW) in order to generate a reactive torque that opposes and is greater than the torque applied on the bicycle by the force of gravity. If the bicycle were falling in the CCW direction then the flywheel (spinning in the same direction) would be gimbaled CW to generate a reactive torque in the opposite direction which in this case opposes gravity. Conversely, if the flywheel were spinning in the opposite direction with its angular momentum pointing towards the positive z-axis the gimbal rotation would be CCW to stabilize a bicycle falling CCW, however changing direction of the flywheel's spin direction will never be utilized because it is not practical to switch the flywheel's rotation direction in a matter of milliseconds to react to a disturbance. Furthermore, a simple static analysis of the bicycle's gyro location and design indicates that the gyro should be placed to minimize the distance between the gyro and the bicycle's to the rotation axis (i.e. the ground). This minimizes the moment arm which gravity will act upon. It is for this reason that most vehicles are designed with a low center of gravity to avoid rolling or losing stability.

2.5.1 **Control Strategy**

In an attempt to generate a basic controller for the system the simplest method of control was taken to be a closed loop sensor feedback PID controller. This type of controller would analyze the system's current angular position, angular velocity, and angular acceleration given by data from accelerometers and inertial measurement units (IMU's). From the sensor feedback the controller would calculate the torque required to exactly oppose the torque generated by the force of gravity acting at the bicycle's center of mass. With this instantaneous and constantly changing value the controller would add a proportional, integral, and derivate gain which would then be fed into the servo motor controller to generate a gimbal behavior (or $\dot{\alpha}$ profile) that would induce a reaction torque larger than the needed torque to merely counteract gravity but rather enough to reverse the acceleration of the bicycle to be in the direction that will bring the bicycle to a stable upright position. The parameters of the servo adjusted by the controller will be the angular velocity $\dot{\alpha}$ of the gimbal and the duration, in time, of the gimbal. After initial free response simulations were conducted for given input gimbal profiles a PID controller was designed and integrated into a Simulink model which generated improved stabilization by reducing settling time and overshoot. Furthermore, Yetkin and Vernier designed a sliding mode controller (SMC), which he validated to be a more robust and accurate controller than the PID controller [13]. An SMC controller is a nonlinear control method that alters the dynamics of a nonlinear system by application of a discontinuous control signal that forces the system to "slide" along a cross-section of the system's normal behavior [14]. The state-feedback control law is not a continuous function of time. Instead, it can switch from one continuous structure to another based on the current position in the state space. Hence, sliding mode control is a variable structure control method [14].

Yetkin's SMC was modeled using the non-linear set of ODE's because of SMC's robust capabilities in handling non-linear systems, where as the simulations this thesis presents were based of the simplified governing equations and assumptions.

To generate a validating MATLAB Simulink model, simplified equations of motion are derived with the stated assumptions in Section 2.3, from the summation of moments about the z-axis due to gravity acting at the bicycles center of mass. By determining the instantaneous required stabilization torque and the instantaneous reaction torque (given an input gimbal rate from the controller) the bicycle's motion and response can be simulated. The torque required or torque due to gravity acting on the un-balanced

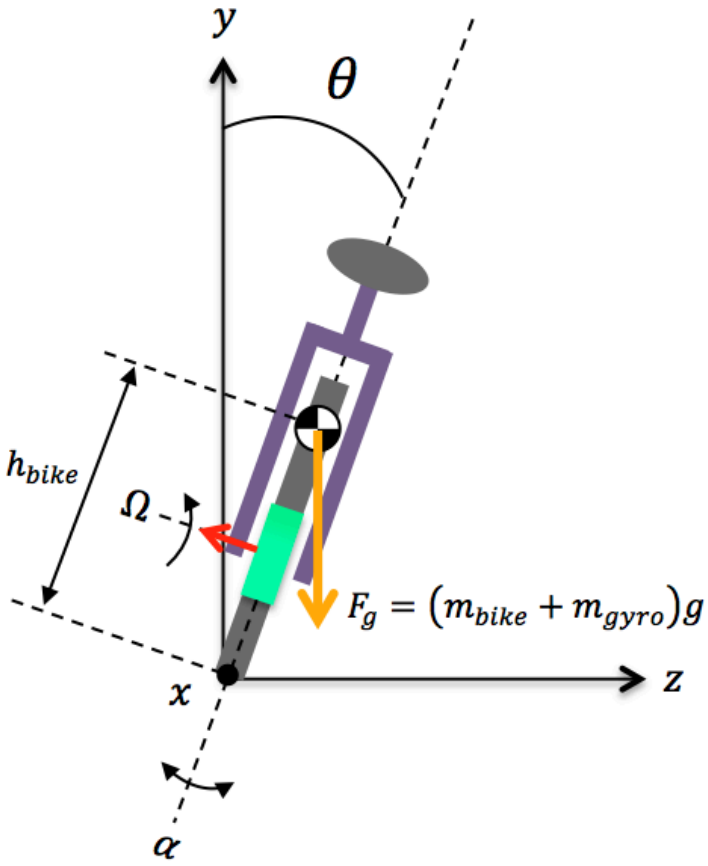

Figure 8: Free Body diagram showing the force due to gravity on the bicycle and the orientation of the flywheel (green) gimbal and spin axes denoted by $\boldsymbol{\alpha}$ and $\boldsymbol{\Omega}$.

bicycle is

$$+\circlearrowleft \sum M_O = \tau_{gravity} = I_{bike}\ddot{\theta}$$

$$+\circlearrowleft \sum M_O = (m_{bike})(h_{bike})g \sin\theta = I_{bike}\ddot{\theta} \quad (8)$$

Now, add a single axis gimbal gyro to the system but assume the gimballing servomotor does not allow the flywheel to precess as the bicycle leans from the vertical (about the z axis). Also assume that the gyro is constrained to rotation about the α axis, which fixed relative to the bicycle.

$$\tau_{gyro} = \Omega\dot{\alpha}m_{fly}r_g^2 = \dot{\alpha}L_g$$

where the above equation is the torque generated by a flywheel with a point mass m_{fly} at the outer radius of the flywheel. The torque generated by gimballing a thin solid disk flywheel is

$$\tau_{gyro} = \left(\frac{1}{2}\right)(\Omega)\dot{\alpha}m_{fly}r_g^2 \quad (9)$$

where the product of $\left(\frac{1}{2}\right)$ is introduced by the centroid of the constant width disk being half that of the point mass which consequently halves the moment of inertia of the flywheel.

Therefore, to stabilize the bicycle (i.e. bring it back to $\theta = 0$), τ_{gyro} must initially be a greater than $\tau_{gravity}$ to generate angular acceleration about point *O* in CCW direction (assuming the bicycle will fall in the CW direction). τ_{gyro} will decrease to zero as θ approaches 0. To maintain or hold the bicycle at a specific θ, $\tau_{gyro} = \tau_{gravity}$. However, as the gyro gimbals the reactive torque acting in about the axis that stabilizes the bicycle decreases to zero as the gimbal angle approaches 90 degrees. To optimize

effective balancing torque output the gimbal angle α should not exceed $\pm 45°$. The equation of the gyro's reactive torque is

$$\tau_{gyro} = \frac{1}{2}\Omega\ \dot{\alpha}\ \left(m_{fly}\right)\left(r_g^2\right)\left[\cos\alpha\ \hat{\imath} + \sin\alpha\ \ \hat{k}\right]$$

$$\tau_{gyro_x} = \frac{1}{2}\Omega\ \dot{\alpha}\ (m_{fly})(r_g^2)\cos\alpha \qquad (10)$$

where,

$m_{fly} = 2\pi r_g^2 w\rho$
$\rho = fly\ wheel\ material\ density$
$w = flywheel\ width$
$m_{bike} = m_{chassis} + m_{hardware} + n\left(m_{fly}\right)$
$n = number\ of\ flywheels$

The component of the reaction torque about the z-axis, noted by $\hat{k}$, can be neglected because the operating angles of the gyro gimbal for stabilization purposes, α, will be within $\pm 45°$. This shows that the torque about the z-axis will always be less than the torque generated about the x-axis until $\alpha = 45°$ where the two components will be equal. The control algorithm to stabilize the inherently unstable body (vehicle or robot) is to control the velocity, $\dot{\alpha}$, of the gimballing actuator to generate an adequate reaction torque capable of opposing gravity's torque on the bicycle. As the bicycle's angular position θ approaches zero the PID output gain generated by the controller on the reaction torque produced should also decrease to a value of 1, which would mean the reaction torque produced was exactly equal to the torque placed on the bicycle by the force of gravity. When the bicycle is in its semi-stable (vertical) position both the required and reaction torques should be zero. The gain profile when tested experimentally can also be adjusted to account for the minor friction losses that were neglected and

assumptions made to simplify the dynamic model. Optimal balancing can be achieved by minimizing both settling time required to reach equilibrium and overshoot.

Therefore it follows that,

$$I_{bike}\ddot{\theta} = \sum M_x = \tau_{gyro_x} - \tau_{gravity} \tag{11}$$

where,

$$\tau_{gravity} = m_{bike}\left(h_{bike_y}\right) g \sin\theta$$

$$\tau_{gyro_x} = \pm\frac{1}{2}\,\Omega\, m_{fly}\, r_g^2\, \dot{\alpha}\cos\alpha$$

$$\therefore \quad I_{bike}\ddot{\theta} = \tfrac{1}{2}\,\Omega\, m_{fly}\, r_g^2\, \dot{\alpha}\cos\alpha - m_{bike}(h_{bike})g\sin\theta \tag{12}$$

$$\text{where } \theta \to 0 \text{ as } \tau_{gyro} \to 0 \text{ and } \tau_{gravity} \to 0$$

2.6 **Maneuverability Algorithm**

As described in the previous section the flywheel or flywheels need to be oriented in a particular initial angular position, $\alpha = 90°$ relative to the initial α for bicycle stabilization, to induce reactive torques about the bicycle's z-axis to maneuver itself into a wheelie position for traversing rugged off-road conditions. The detailed design of a gyro system will be explained in Chapter 4, however a brief analysis will be conducted to determine the basic orientation of the gyros for inducing wheelies. The gyro capable of stabilizing the bicycle was constrained to one rotational degree of freedom about the y-axis shown in Figure 12. Similarly, this constraint is still necessary in the system that is capable of inducing wheelies. However, the difference now is that the initial orientation of the flywheel will have the flywheels angular momentum point to either the positive or negative x-axis as opposed to the z-axis for balancing. This orientation will allow the

flywheel, when gimbaled CCW, to generate a torque about the z-axis, which will act to lift the bicycles front tire off the ground and the rear, tire into the ground (or vice versa if the gimbal was CW).

3 Bicycle Prototype Platform: Balancing

3.1 Gyro Mechanical Design

The design of a single-axis gimbal control moment gyroscope is composed of several mechanisms and mounting structures. A single-axis gimbal CMG has 2 degrees of freedom: one rotational degree of freedom for the flywheel to spin about its spin axis, and another rotational degree of freedom for gimballing, which is rotation about an axis orthogonal to the spin axis. To maximize the effectiveness of the CMG multiple parameters need to be optimized. From Eq. 10 it is evident that the reactive torque produced by the CMG is dependent on several design parameters of the flywheel, mainly the flywheel's mass and radius. The mass of the flywheel is a function of the flywheel's geometry as well as the material used. The reactive torque produced by the CMG is linearly proportional to the mass of the flywheel and quadratically related to the radius of the flywheel from the reaction torques dependency on the flywheel's moment of inertia. As either of these parameters increases the maximum reactive torque capable of being produced also increases for a given flywheel spin speed (Ω) and gimbal speed ($\dot{\alpha}$).

3.1.1 Flywheel Optimization

To optimize the output reactive torque produced by the single-axis gimbal CMG the flywheel's radius and mass needed to be optimized. Because the bicycle's total weight is dependent on the mass of the flywheel, as the flywheel increases in size and weight the bicycle also increases in weight, which therefore would require a greater torque to stabilize itself. Therefore, MATLAB code was written to optimize the flywheel

output torque while minimizing the required torque to stabilize the bicycle given an initial perturbation angle from the semi-stable position (i.e. $\theta = 0$). Figure 9 shows the results of the optimization program, which suggests that the optimal steel flywheel within the design space would have a radius of 6 cm with a width of 3.2 cm. The flywheel can be optimized further by designing a unique flywheel geometry profile. A constant width disk is used for the prototype because of the fabrication costs associated with machining a non-constant width disk while ensuring minimal mass imbalance, which would pose potential problems at operating angular velocities as high as 20,000 rpm. However, if the budget were not a factor, the optimal flywheel geometry would have the majority of its mass located towards the outside radius of the flywheel (approaching a point mass ring geometry) and a thin, possibly spoked or ribbed, cross section towards the flywheel's center. This design would maximize the flywheels moment of inertia because the moment of inertia equation for a point mass, with radius 'r' from the axis of rotation, is $I_{point} = mr^2$, where the moment of inertia for a constant width disk is $I_{disk} = \frac{1}{2}mr^2$. Therefore, the disk flywheel moment of inertia is half that of the point mass, which

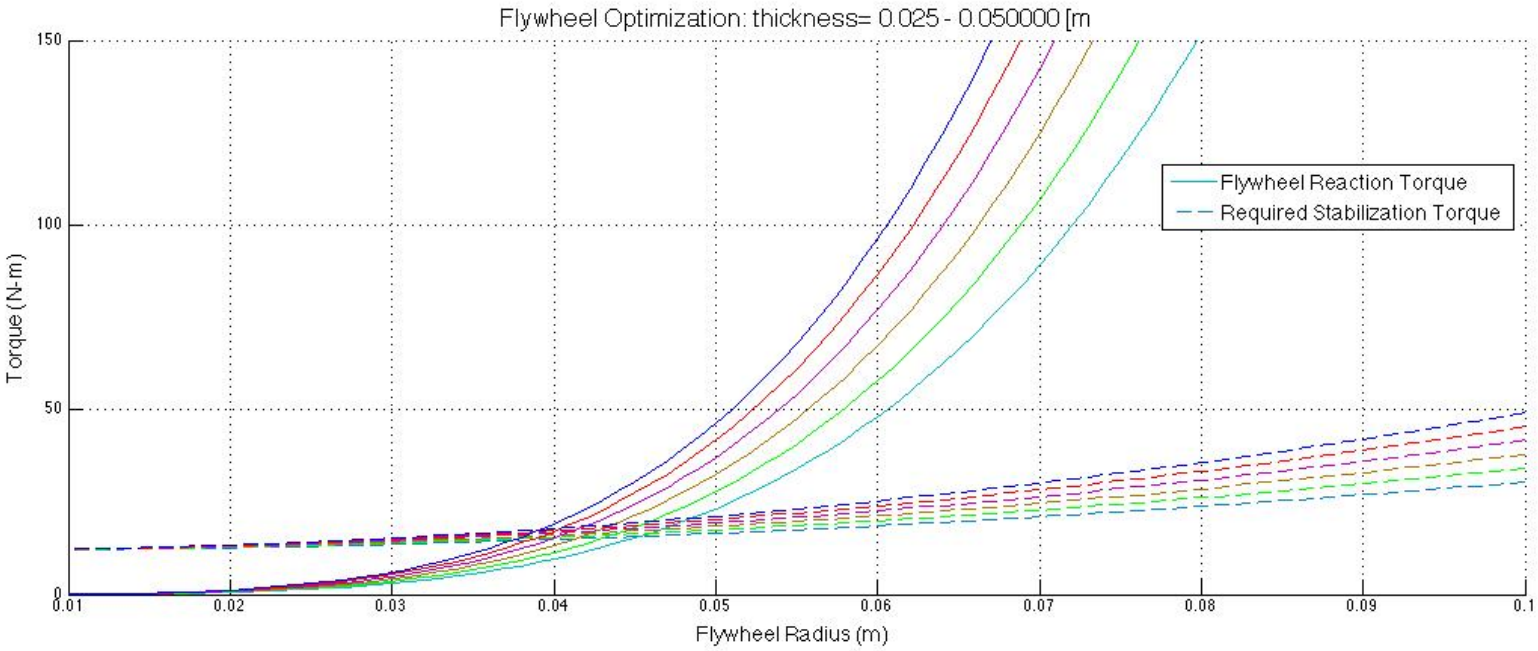

Figure 9: MATLAB optimization plot of a steel flywheel's radius and width with respect to flywheel's output reactive torque and bicycle required torque. Thickness increase from .025 m to .05 m by .005 m from light blue, green, yellow, magenta, red, to dark blue.

means that a flywheel with the majority of its mass located on the outside radius will have a larger moment of inertia and consequently produce more reactive torque than a constant width disk flywheel. Flywheel mass is a function of the radius, width, and density of the material being used. Therefore finding the optimal mass for a given geometry (radius and width fixed) will determine what approximate density is needed and from that an appropriate metal can be used. Optimization design calculations were conducted on a steel, 1090 mild ($\rho_{st} = 7850\frac{kg}{m^3}$), flywheel as well as a tungsten ($\rho_{tung} = 19600\frac{kg}{m^3}$) flywheel. Optimization is required because although there is a naturally existing limit to the maximum density of available materials, as the density of the material increases the tensile stress (primary failure mode for flywheels) on the flywheel also increases linearly. For the steel flywheel the optimal design parameters were found to be a radius of 6 cm and a width of 3.2 cm (within bicycle's design space). A steel flywheel with this geometry would produce $\tau_{gyro} = \tau_{gyro}(\dot{\alpha}) = 10.71 * \dot{\alpha}$ N-m of reactive torque when it would need 20.48 N-m of torque to counteract the torque due to gravity at an initial perturbation angle of $\theta = 20°$. The plots in Figure 10 signify that the

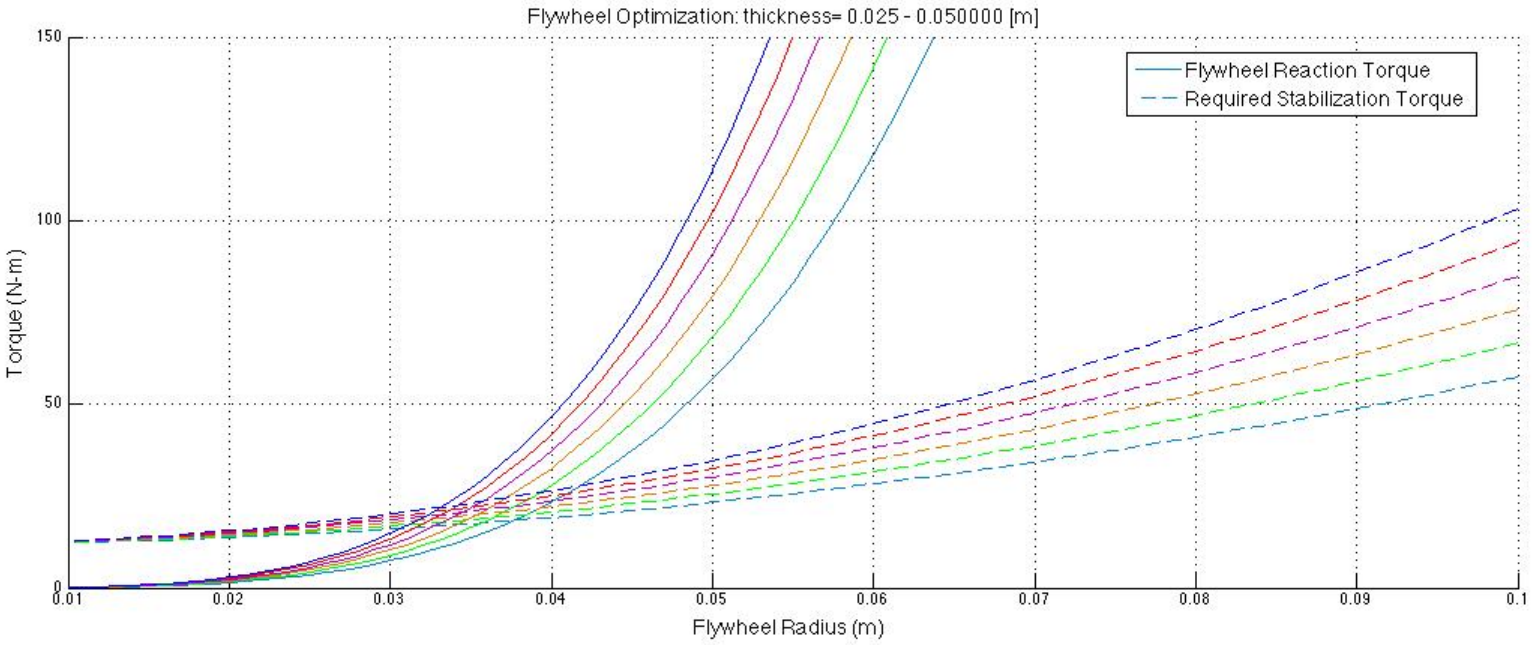

Figure 10: MATLAB optimization plot of tungsten flywheel's radius and width with respect to flywheel's output reactive torque and bicycle required torque. Thickness increase from .025 m to .05 m by .005 m from light blue, green, yellow, magenta, red, to dark blue.

required torque to balance the bicycle varies minimally with the increasing flywheel parameters. This is in part due to the fact that the flywheel accounts for only 16% of the bicycles total weight. Alternatively, the tungsten flywheel can generate a much larger reactive torque than a steel flywheel but the added weight of the flywheel increases the required torque more drastically because the tungsten flywheel would account for nearly 29% of the total bicycles weight. The tungsten flywheel torque output plot is shown in Figure 10. A tungsten flywheel of the same geometry can produce $26.26 * \dot{\alpha}$ N-m of reactive torque.

Due to the mass of the flywheel accounting for between 15% and 30% of the bicycles total weight (respectively to the material used) the location of the flywheel on the frame of the bicycle also needs to be optimized to minimize the required torque to stabilize the bicycle. The bicycle frame had 2 adequate locations on which a flywheel could be mounted: one at the top of the frame near the seat or one below the frame, level with where the pedals would be. Of the two locations the lower location is much more advantageous because the added weight towards the bottom of the bicycle would lower the bicycles center of gravity which is directly related to a vehicles lateral stability. This can be understood by observing the following equation, which models a bicycles behavior in response to purely the force of gravity.

$$+\circlearrowleft \sum M_O = \tau_{gravity} = (m_{bike})(h_{bike})g \sin\theta = I_{bike}\ddot{\theta}$$

where, h_{bike} is the distance from the ground to the bicycle's center of gravity. Therefore the higher the bicycle's center of gravity is (i.e. the greater h_{bike} is), the larger the torque due to gravity will be which will require a greater gyro reaction torque to stabilize the bicycle, which is not desired.

3.1.2 **Flywheel Design Considerations**

It is worth considering that as the density of the flywheel increases (steel to tungsten) the centrifugal force, responsible for the main failure mode of flywheels at high rpm's, also increases significantly. The centrifugal force (F_c) can be calculated as,

$$F_c = mr\omega^2$$

where the stress acting on the flywheel is calculated by the following equations. The calculated stress must not exceed the flywheel's ultimate tensile stress or catastrophic failure in the flywheel will occur by fracture and bursting [15] [16].

$$\sigma_{fly} = \frac{1}{2}\rho\omega^2 r^2 = \frac{1}{2}\left(7850\,\frac{kg}{m^3}\right)\left(20000\left(\frac{2\pi}{60}\right)\frac{rad}{s}\right)^2 (.06\ m)^2 = 61.98\ MPa \quad (13)$$

$$\therefore\ \ \sigma_{max} = 400\ MPa\ > \frac{1}{2}\rho\omega^2 r^2$$

$$n_{d,Steel} = \frac{\sigma_{max}}{\sigma_{fly}} = \frac{840}{61.98} = 13.55$$

$$n_{d,Tung} = \frac{\sigma_{max}}{\sigma_{fly}} = \frac{1510}{152} = 9.93$$

The design calculations show that although both flywheels would be safe at this applications operating velocity the steel flywheel has a greater factor of safety. Also, it is typically standard procedure to enclose a high rpm flywheel in a burst proof chamber in the case that the flywheel failed and burst catastrophically to avoid the obvious harm that could create. However, because the factor of safety for the maximum operating conditions of this flywheel was upwards of 10 the flywheel was not enclosed in a chamber to save costs.

To maximize the energy efficiency of a flywheel the losses due to air resistance and friction must be minimized. To completely minimize the energy due to air resistance losses the flywheel can be enclosed within a vacuum chamber. To determine the effectiveness of housing the flywheel in a vacuum chamber the following set of

equations was used to determine the percent of energy lost due to air resisting the flywheels rotation [17].

$$T_{air} = \rho_{air} r^5 \omega^2 C_m \tag{14}$$

where,

$$C_m = f(R_e) = 3.87 R_e^{-\frac{1}{2}}$$

$$R_e = \frac{\rho_{air} \omega r^2}{\eta}$$

$$\eta \cong \frac{1}{2} \rho_{air} \bar{v} \lambda$$

$$\bar{v} = \sqrt{\frac{8kt}{\pi m}}$$

$$\lambda = \frac{m}{a^2 \rho_{air} \pi \sqrt{2}}$$

Comparatively, the losses due to Roller bearing friction can be calculated via the following set of equations [18].

$$f_{bearing} = \mu F_R \tag{15}$$

$$T_f = f_{bearing} * \frac{d_{bore}}{2} = \mu F_r \left(\frac{d_{bore}}{2}\right)$$

where,

$$F_R = radial\ force = m_{fly} * g$$

$\mu = 0.0015$ *for a single row ball bearing with radial loads* [18].

Therefore the total torque opposing the flywheel's rotation due to both air resistance and roller bearing friction is calculated by,

$$T_{losses} = T_{air} + T_f$$

$$\sum M_o = T_{motor} - T_{losses} = I\ddot{\alpha} = \frac{1}{2} m_{fly} r^2 \ddot{\alpha}$$

$$T_{losses}(2\pi\Omega) = P_{loss}\ [watts]$$

$$\frac{E_{loss}}{E_{flywheel}} = \frac{(T_{air}+T_f)(2\pi\Omega)}{\frac{1}{2}I\omega^2} \quad (16)$$

Another geometric characteristic worth optimization is the energy density of the flywheel. The two parameters most responsible for optimizing a flywheel's energy density are the flywheel geometry and the flywheel material [19].

$$\frac{E}{m} = K\left(\frac{\sigma}{\rho}\right) \quad (17)$$

where,

$E - kinetic\ energy\ of\ the\ flywheel\ [J]$
$m - flywheel\ mass$
$K - flywheels\ geometric\ shape\ factor = .606$ (for constant thickness disc geometry)
$\sigma - tensile\ strength\ of\ the\ flywheel\ material\ [Pa]$

$\rho - materials\ density\ \left[\frac{kg}{m^3}\right]$

3.1.3 Electronics: Actuators, Sensors, Micro-controller

Figure 11 is a schematic system diagram of the electronic components and sensors interconnections on the bicycle setup. Solid lines in the diagram represent a physical connection between components while dashed lines indicate that there is no physical connection between components but that state of one component affects the other. Similarly, the box representing the bicycle (Pendulum Orientation) is dashed, meaning that the pendulum's orientation is not a physical component but rather it is a parameter that affects and is affected by the components it is connected to it. The diagram identifies data acquisition components or sensors in blue, power sources (LiPo batteries) in red, and actuators/motors in green [13].

Therefore the system operates to stabilize the bicycle in a manner of executing a few tasks [13]:

- The flywheel is set to spin at a constant angular velocity

- The tilt angle of the bicycle is instantly measured by the Inertial Measurement Unit (IMU)
- The IMU data is read by the Arduino micro-controller
- The measured tilt angle is acquired by Beaglebone from the IMU through USB interfacing
- The gimbal servo motor is actuated as determined by the closed loop feedback controller

The self-balancing bicycle gyro system is composed of only two actuators (for a static bicycle). A brushless DC hobby motor is used with an electronic speed controller (ESC) to spin the flywheel up to around 10,000 to 20,000 rpm. This motor has its own control loop. Once the flywheel reaches a specified constant speed, the motor only provides additional torque to overcome losses from air resistance/drag and bearing friction. The second actuator uses is a DC servomotor coupled to the flywheel's orthogonal axis, which is used to actuate the gimballing mechanism of the flywheel. The

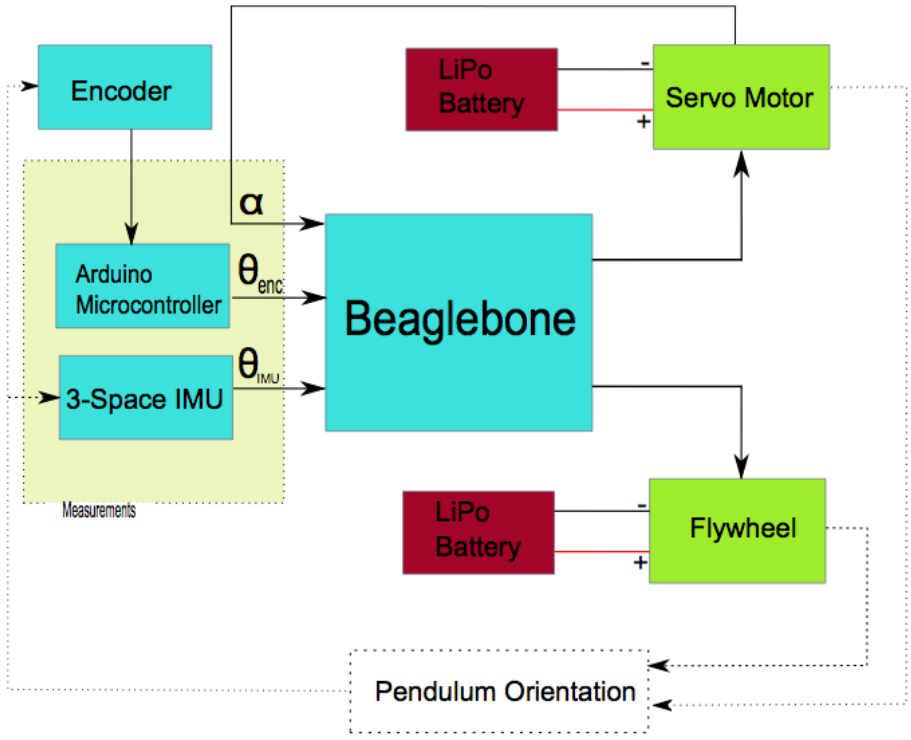

Figure 11: Component and parameter interconnections schematic. The bicycle orientation or angle $\boldsymbol{\theta}$ is labeled pendulum orientation and the inertial measurement unit (IMU) is labeled encoder [13].

servomotor used is a Trossen Robotics Dynamixel EX-106+ series robot servo actuator.

Table 2: Dynamixel EX-106+ Specifications

Dynamixel EX-106+ Spec	14.7 V	18.5 V
Encoder Position	.06° resolution over 250°	
Gear Reduction Ratio	184:1	
Feedback	Position, temperature, load, input voltage	
Rated Holding Torque	8.24 [N-m]	10.5 [N-m]
Tested Holding Torque		12.76 [N-m] @ I=1.14 [A]
No-load Speed	5.75 [rad/s]	7.32 [rad/s]
Max current		7 [A]

Two lithium polymer (LiPo) batteries were used to power the two actuators. A 6-cell (6s), 22.2 V LiPo was used to power the flywheel spinning brushless DC motor and a 4-cell (4s) 14.8 V LiPo was used to power the Dynamixel gimballing servomotor.

3.1.3 CAD Renderings and Fabrication

In order to design a gyro constrained to just one revolute degree of freedom (DOF), a gimballing mechanism (shown in Figure 12 and Figure 15) was created. The Dynamixel servomotor (beige) is coupled, via a misalignment shaft coupler (red), to a

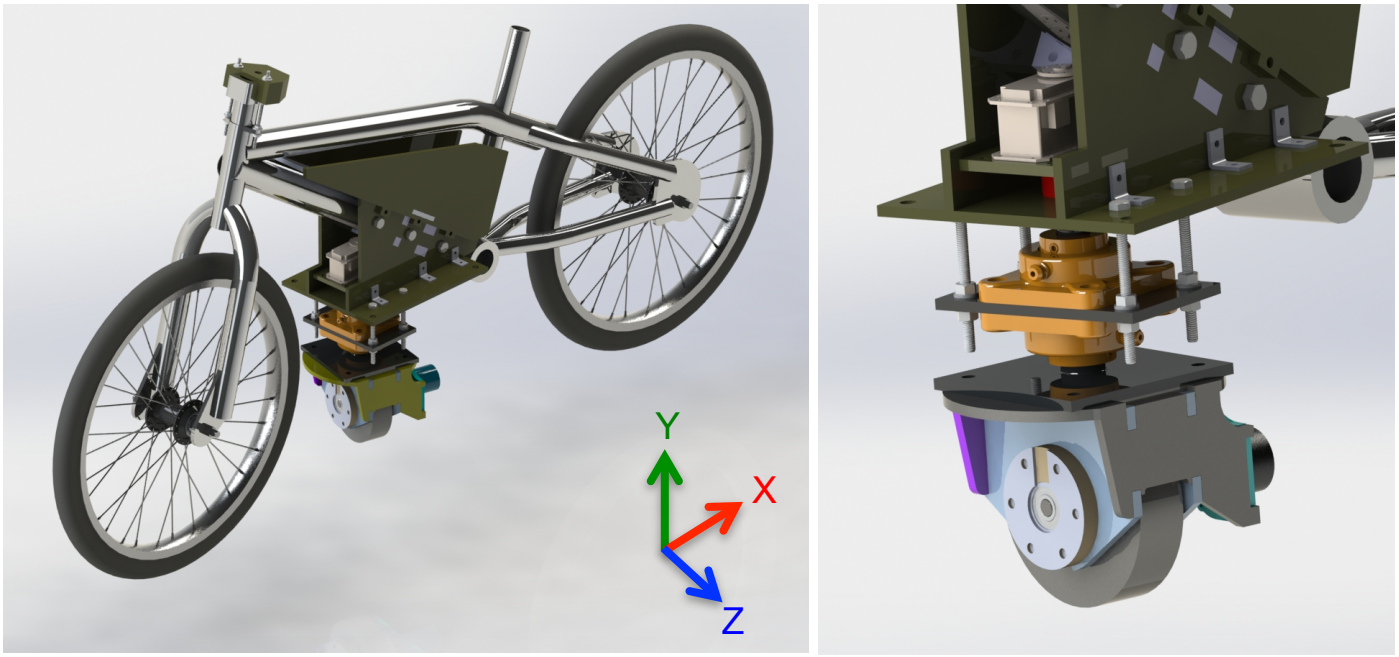

Figure 12: Complete self-balancing bicycle design with all single-axis gimbal gyro mechanical components assembled (left). Close up view of the gyro and gimballing mechanism (right).

shaft, which was welded to a plate with a bolt pattern identical to that on the base of the gyro's housing. The shaft passes through two misalignment bearings (yellow), which constrains the shaft from rotation about the x and z-axes and translation about the x, y, and z-axes relative to the bicycle frame. A plate was used to mount the bearings to, which then was fixed via 4 threaded rods and nuts, to the main mounting structure. The main mounting structure was fabricated using 0.25" laminated plywood sheets (green) which were all laser cut fabricated. The mounting structured is fastened rigidly to the bicycle frame's down tube via 3, 3/8" bolts and a series of laminated plywood tube collars designed as additional supports to minimize slop in the structure. Furthermore, an additional laminated plywood structure between the top and bottom bicycle tubes was added to mount on-board electronic components, controllers, and batteries. A steering lock structure was designed to fix the steering wheel from rotating during static testing.

A close up of the actual flywheel assembly with motor, rotor, coupling, bearings, and housing can be found in Figure 13.

3.2 Modeling and Simulations

Using Eqn. 12, a simplified governing ODE for the bicycle's motion, MATLAB code was written to observe the system's response. The input to the system is $\dot{\alpha}$, which will be the output of the designed PID controller. The bicycle's set parameters and

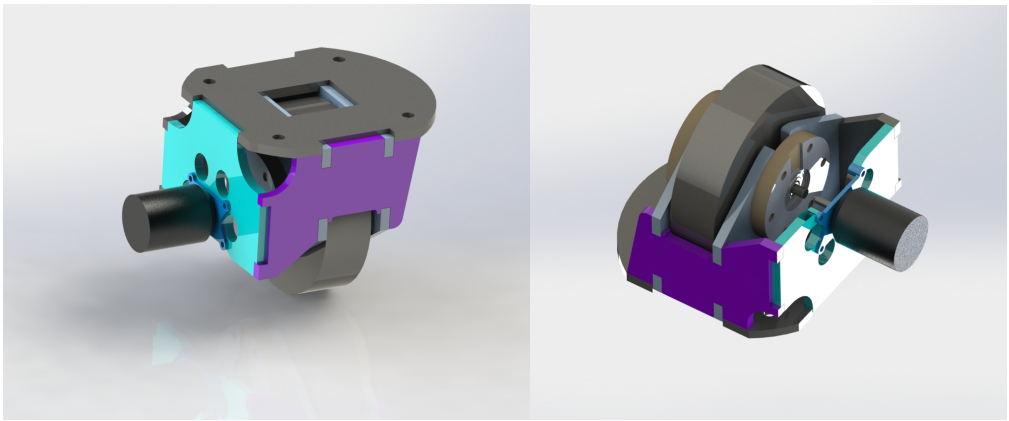

Figure 13: Flywheel assembly with all components and motor shown. Base plate mounts to gimbal shaft via the 4-hole bolt pattern (left).

constants can be found in the code listed in Appendix B and in Table 3. These parameters are based off of the physical bicycle prototype that was constructed. Several scenarios with different bicycle initial conditions and disturbances, $\theta \text{ and } \ddot{\theta}$, were simulated to determine the unique gimbal profiles required to stabilize the bicycle.

3.2.1 **Simulink Stabilization Model**

A Simulink model was generated using the simplified ODE and a PID controller was designed to take an input of a desired bicycle angle θ, which would be set to zero (semi-stable, vertical position) for most scenarios. A simulation was also done on an input of $\theta = 10°$ to emulate dynamic turning capabilities where the bicycle would be tilted when turning similarly to when a human rider leans to turn on a bicycle. Simulation tests where also conducted to determine what maximum initial angle θ the bicycle could stabilize itself from with the designed gyro system. The output of the PID controller is $\dot{\alpha}$, which the reaction torque of the gyro is directly dependent on. The PID controller was designed and tuned accordingly to have coefficients $P = 12,\ \ I = 15,\ \ D = 1$, which reduced overshoot and minimized settling time of the response. The controller was also designed to have the gimbal angle, α, return to its initial angle, $\alpha_o = 0°$, so that after stabilizing the bicycle's initial perturbation the gyro would be in its most optimal position to handle a second disturbance and similarly continue to handle multiple more disturbances. If the gimbal angle, α, were not returned to zero after stabilizing the bicycle then the gyro would not be capable of producing its maximum reaction torque for the next disturbance introduced into the system which could possibly not be enough to stabilize the bicycle. The Simulink model was generated based off of Eqn. 18 and the PID controller equation is shown in Eqn. 19.

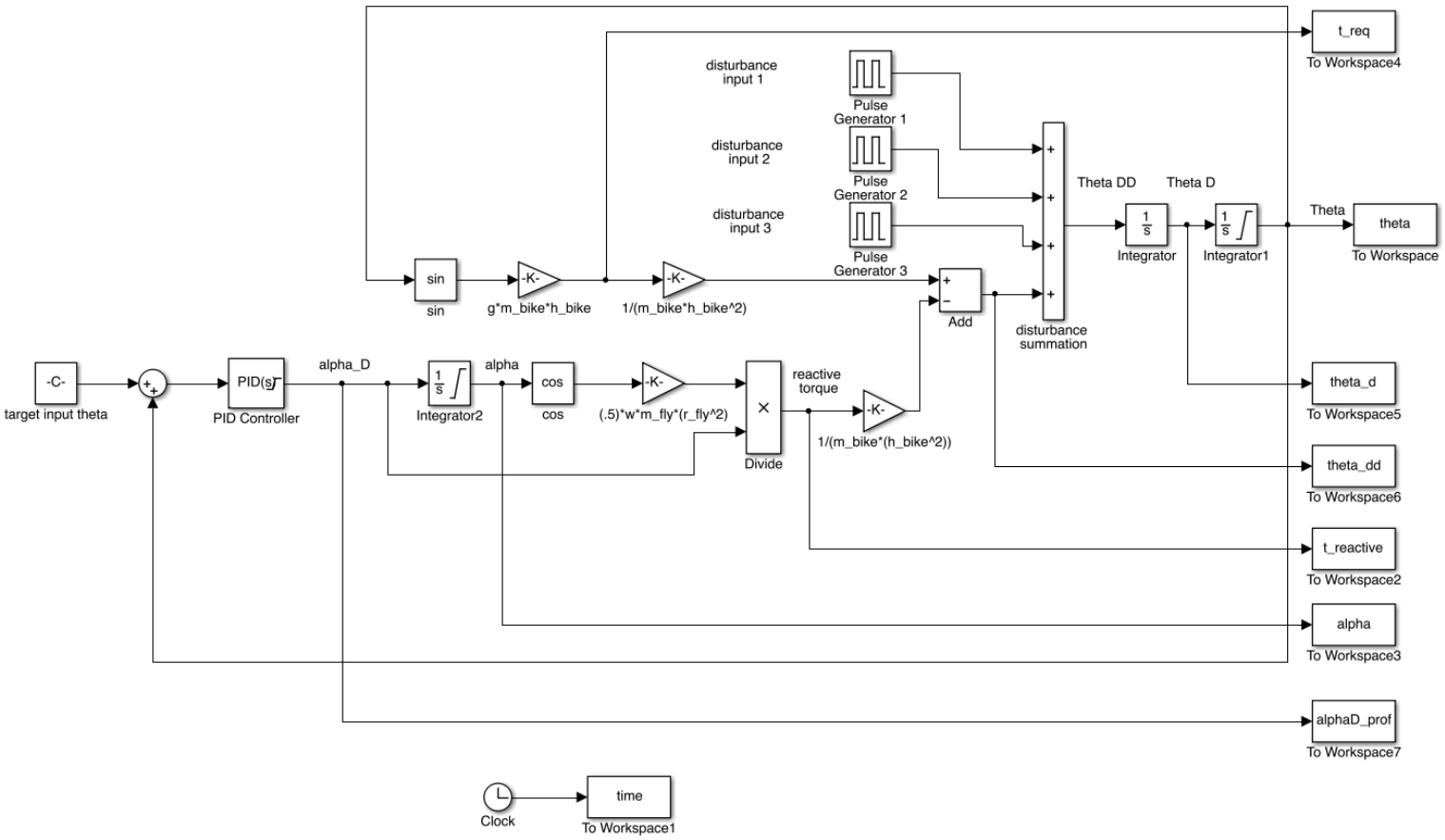

Figure 14: Simulink model for bicycle dynamics and PID controller system response

$$\ddot{\theta} = \frac{\frac{1}{2}\,\Omega\, m_{fly}\, r_g^2\, \dot{\alpha}\cos\alpha - m_{bike}(h_{bike})\, g \sin\theta}{I_{bike}} \tag{18}$$

$$\text{PID Controller: } P + I\frac{1}{s} + D\frac{N}{1+N\frac{1}{s}} = 12 + (15)\frac{1}{s} + (1)\frac{N}{1+N\frac{1}{s}} \tag{19}$$

The generated Simulink model is shown in Figure 14. This model was used to generate the system response plots and calculate the instantaneous angles θ, α, the required torque versus reaction torque, the bicycle angular velocity, $\dot{\theta}$, angular acceleration $\ddot{\theta}$, and the gimbal angular velocity profile which is the output of the PID controller. Voltage control on the gimbal servomotor can replicate the simulated angular velocity gimbal profile generated by this model's PID controller for the actual prototype experimental testing. The gimbal angular velocity PID output is limited to the maximum

load bearing physical angular velocity of the Dynamixel servo to ensure the PID controller creates a gimbal profile that the Dynamixel servomotor can execute accurately.

To simulate the gyro's stabilization capabilities the first simulation conducted had the bicycle starting at an initial offset or perturbation angle of $20°$ and initially at rest (i.e. $\theta_i = 20°$ and $\dot{\theta} = 0$). Figure 16 shows that the PID controller generates a feasible gimbal velocity profile that stabilizes the bicycle (i.e. brings θ back to zero) in just 1-2 seconds. It can also be noted that the PID controller brings the bicycle back to $\theta = 0$ while also having $\dot{\theta} = \ddot{\theta} = 0$ which is ideal for balancing and physically means that the bicycle approaches its semi-stable position and when it reaches it the bicycle's angular velocity and angular acceleration are also zero. This means the bicycle is in its most stable state as opposed to just passing through the semi-stable position and not stopping at it. Also worth noting is the fact that the PID controller brings α back to zero when the bicycle reaches its vertical position.

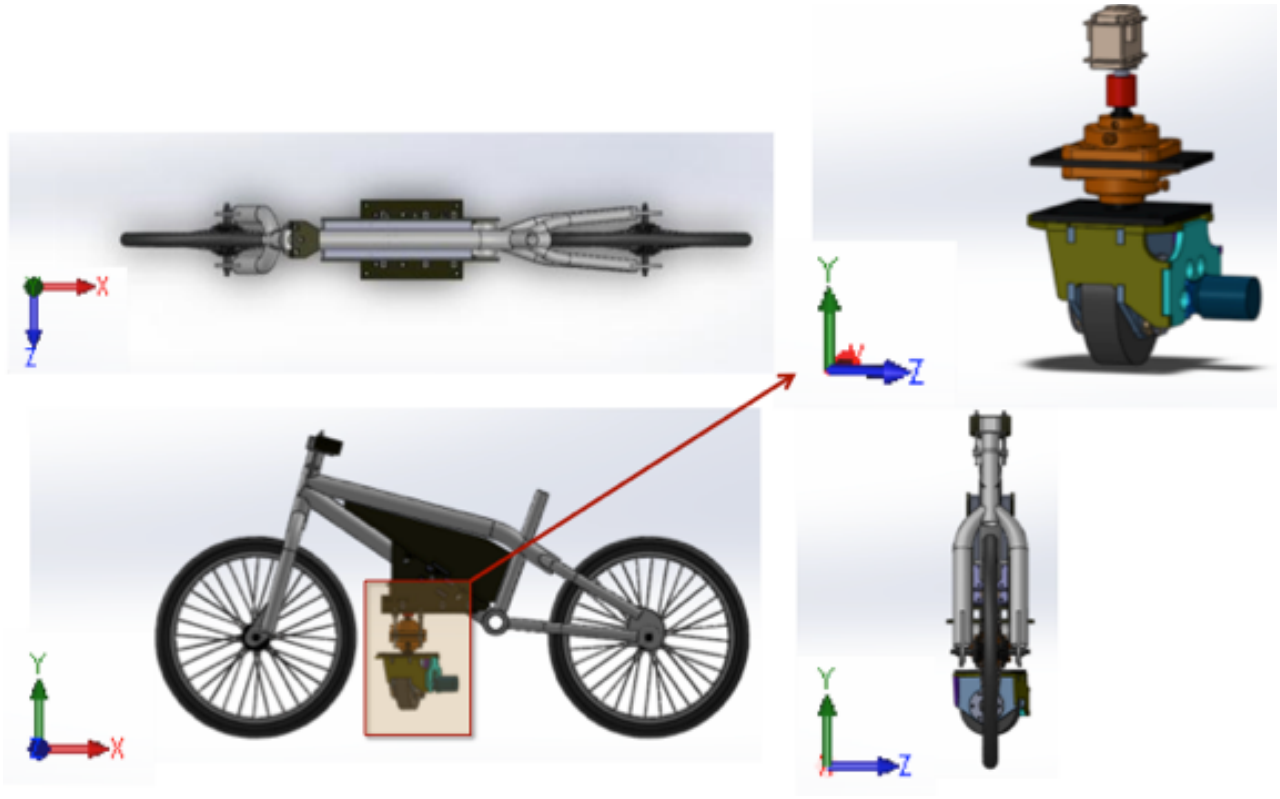

Figure 15: Single axis CMG shown mounted to bicycle via mounting hardware, pair of gimbal bearings, and servo motor gimbal actuator.

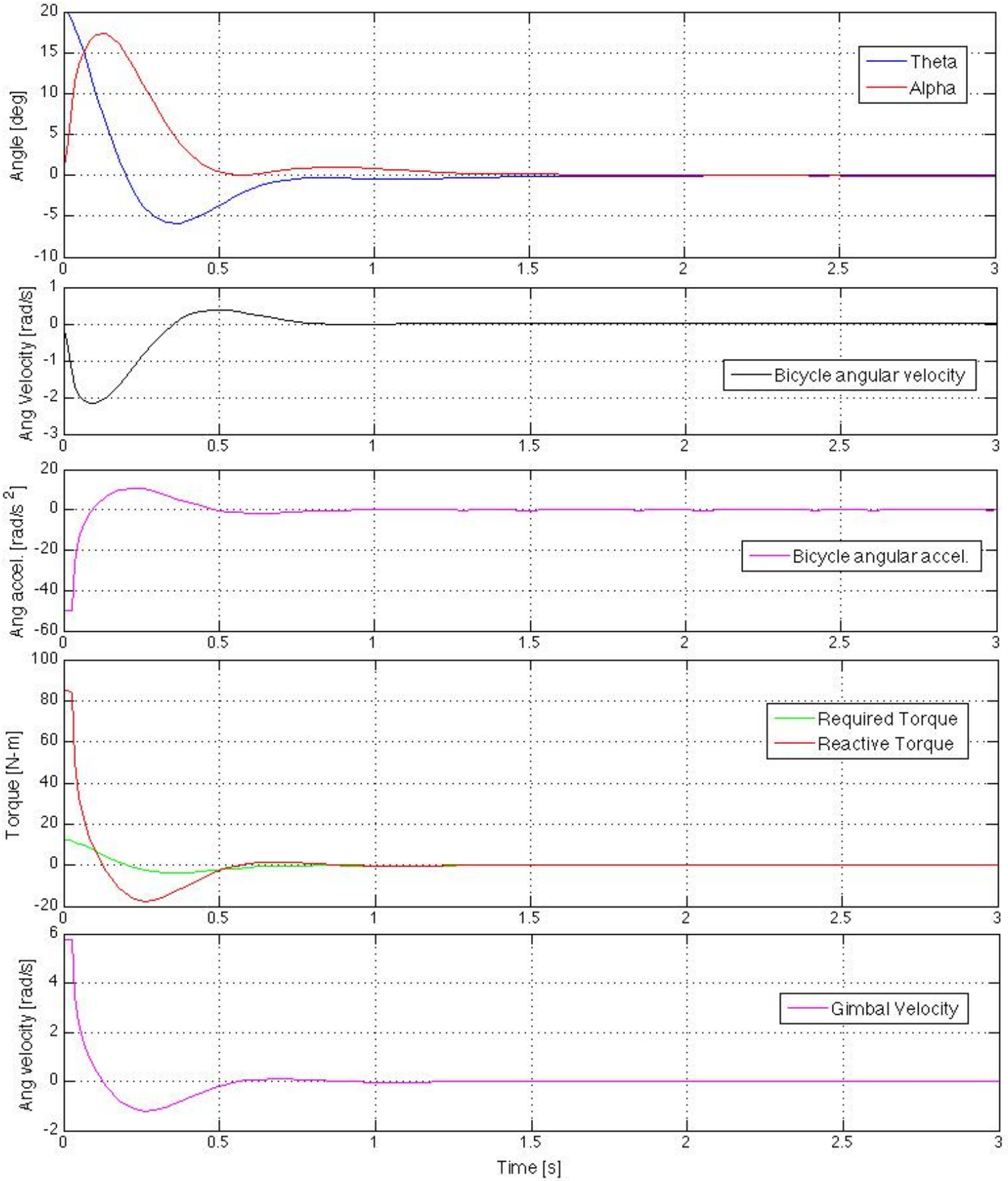

Figure 16: Simulation plots of bicycle with initial conditions $\boldsymbol{\theta} = \mathbf{20}$ and $\dot{\boldsymbol{\theta}} = \mathbf{0}$. Bicycle Angle and Gimbal angle plot (top). Bicycle angular velocity (2^{nd} from top). Bicycle angular acceleration (3^{rd} from top). Required and Reactive torques (4^{th} from top). Angular Velocity, $\dot{\boldsymbol{\alpha}}$, gimbal profile (bottom)

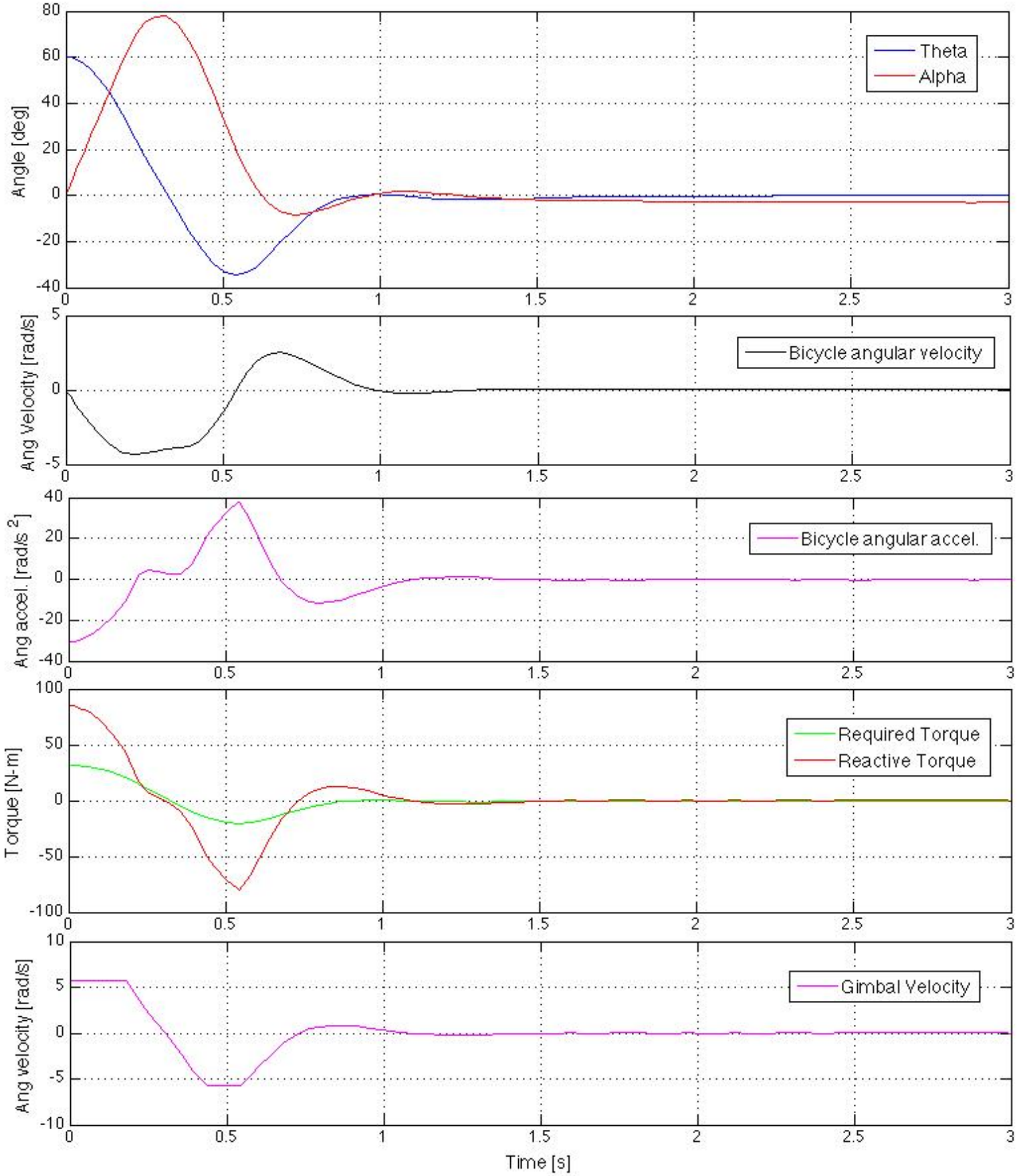

Figure 17: Simulation plots of bicycle with initial conditions $\boldsymbol{\theta} = \mathbf{60}$ and $\dot{\boldsymbol{\theta}} = \mathbf{0}$.

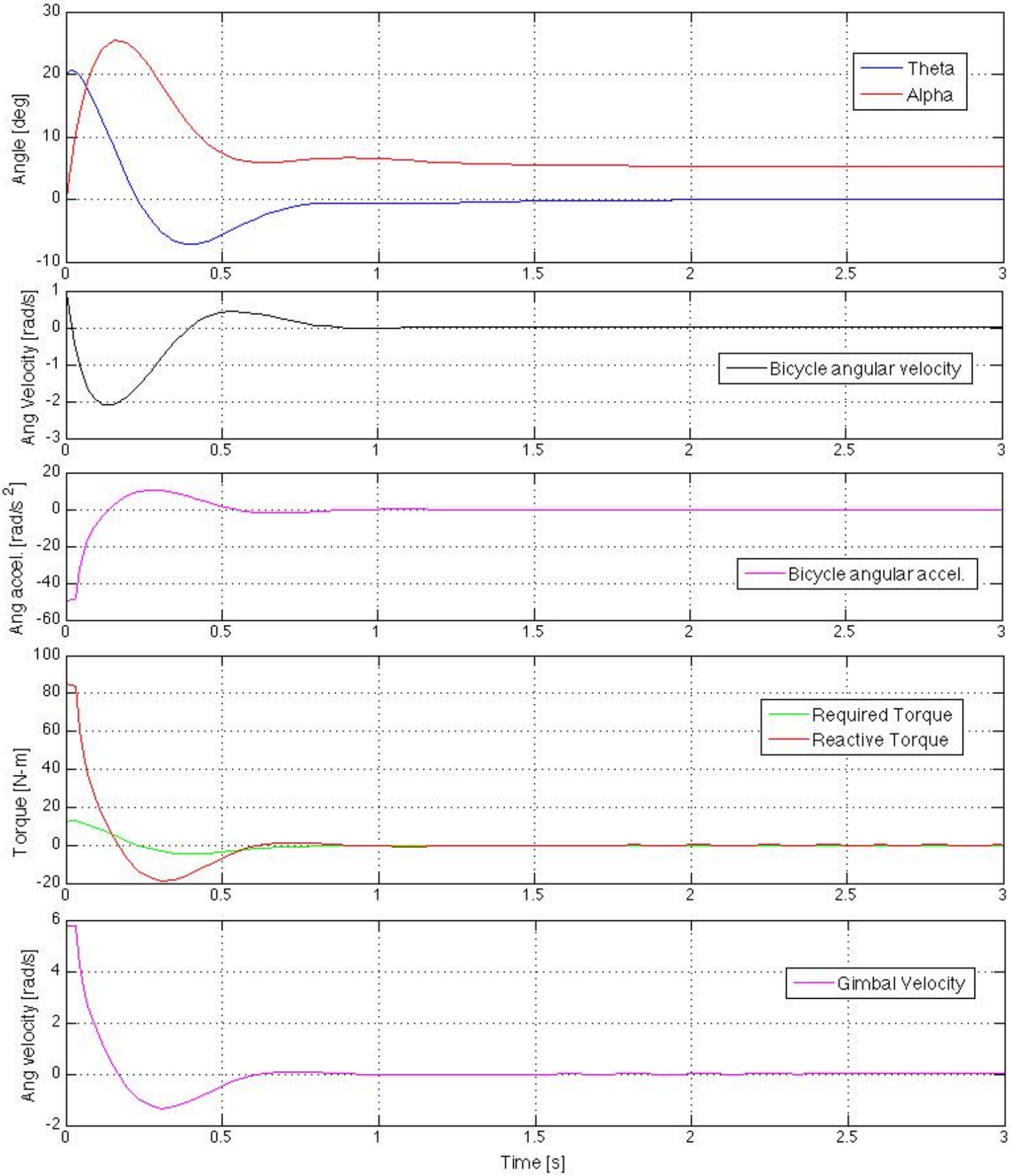

Figure 18: Simulation plots of bicycle with initial conditions $\boldsymbol{\theta} = \mathbf{20}$ and $\dot{\boldsymbol{\theta}} = \mathbf{1}\ [\frac{\boldsymbol{rad}}{\boldsymbol{s}}]$.

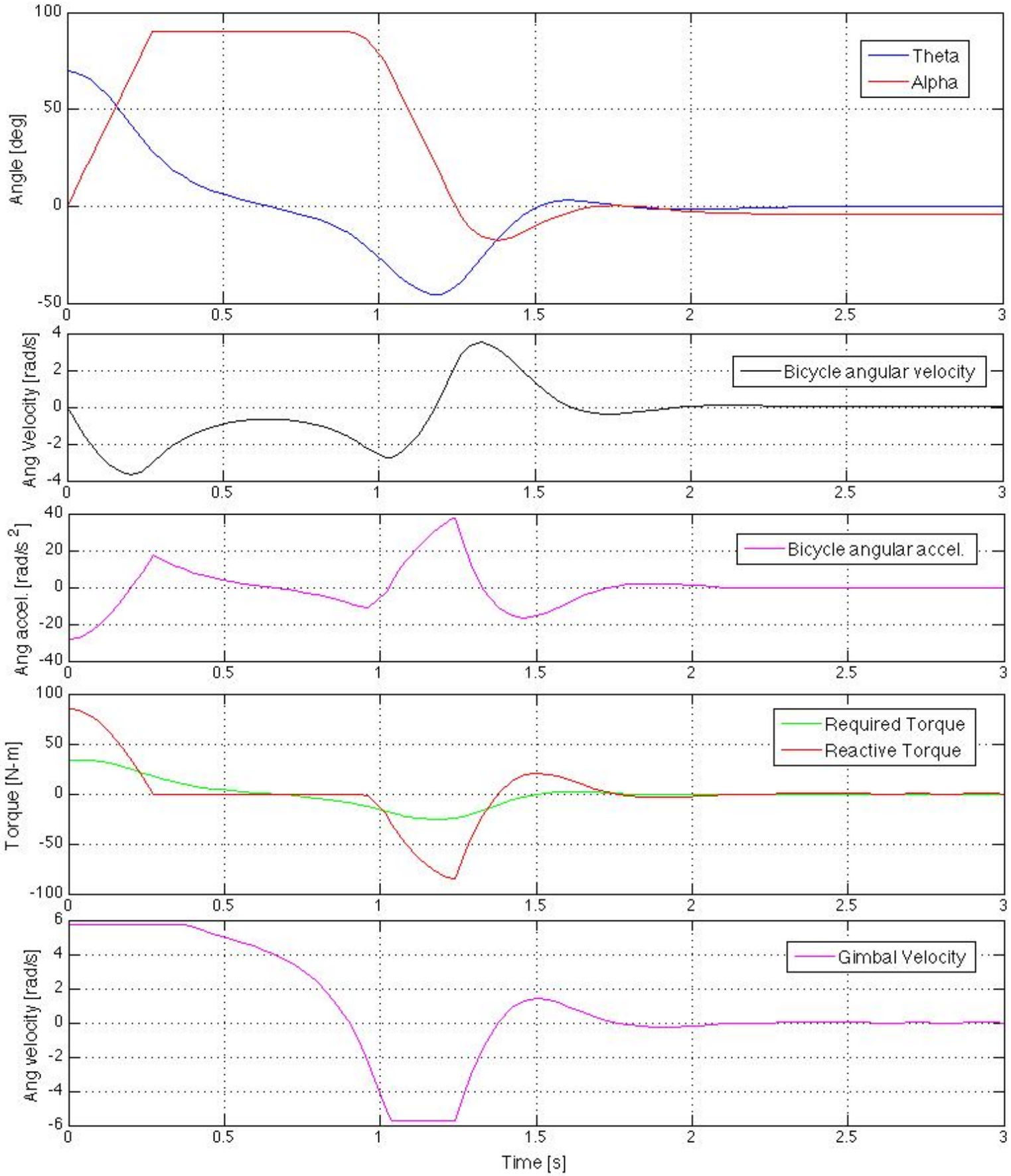

Figure 19: Simulation plots of bicycle 'wake up' maneuver which is when the bicycle starts with initial angle close to $\boldsymbol{\theta = 90°}$ which emulates a scenario where the bicycle or vehicle would be on its side initially then stand up using the gyro. Exact initial conditions of the simulation are $\boldsymbol{\theta = 69}$ and $\boldsymbol{\dot{\theta} = 0}$ where are $\boldsymbol{\theta = 69}$ is the largest initial perturbation angle that the bicycle can recover from with this designed gyro system.

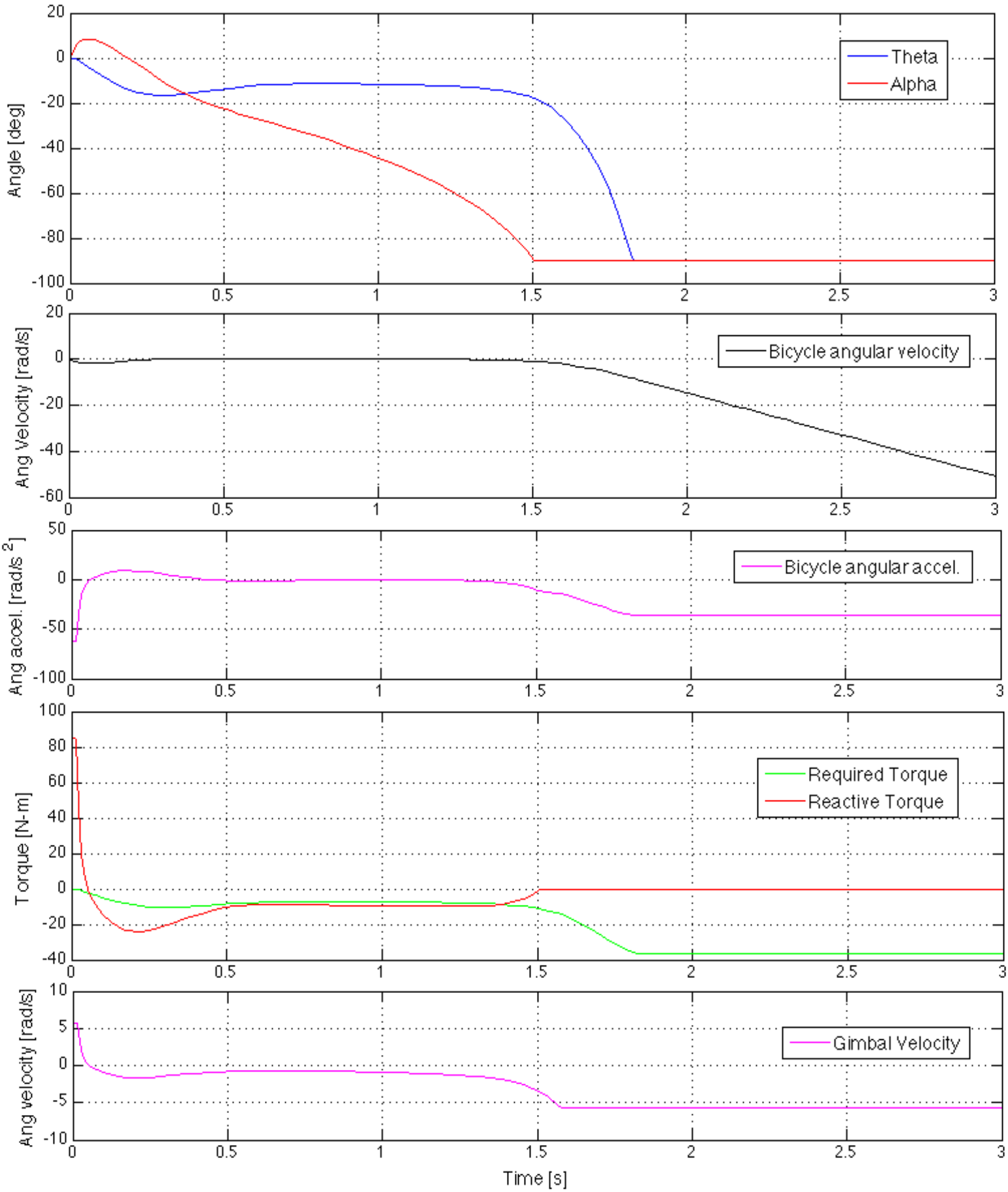

Figure 20: Simulation plots of bicycle with initial conditions $\boldsymbol{\theta} = \mathbf{0}°$ and $\dot{\boldsymbol{\theta}} = \mathbf{0}$ where the input theta to the controller is $\mathbf{10}°$. This type of scenario would emulate a dynamic condition where the bicycle may be turning and therefore a lean or tilt of around $\mathbf{10}°$ in the bicycle would be necessary. This control can also be used in advanced maneuvering situations.

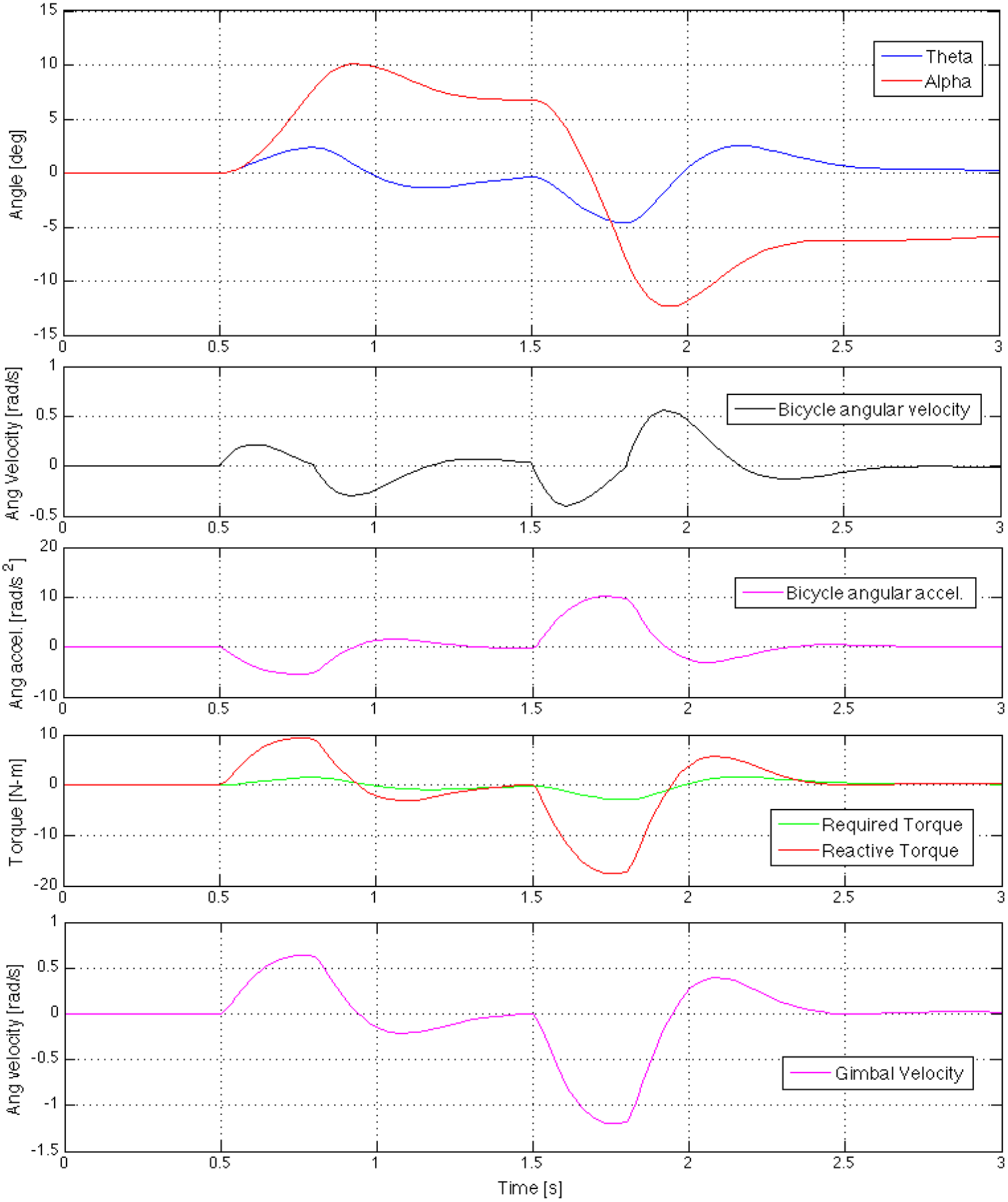

Figure 21: Simulation plot where bicycle is stable until an initial disturbance is introduced at t=0.5 sec and then a second disturbance at t=1.5 sec. The disturbance comes in the form of a force applied at a distance from the bicycles pivot (where wheels touch ground) which produces a net external torque and consequently an angular acceleration $\ddot{\theta}$

3.2.2 **Simulation Results and Analysis**

The Simulink model created was based off the simplified governing equation of motion derived from the summation of moments acting about the bicycle's x-axis. The physical and control operating parameters for the gyro system used in all the simulations can be found in Table 3. The gimbal velocity $\dot{\alpha}$ was limited to slightly less than the servomotors max velocity by the PID controller to ensure that the controller wouldn't generate a response that the physical system was not capable of executing. The Simulink model was very robust in allowing a variety of initial conditions to be set and tested in addition to its ability to introduce disturbances at any time in the simulation. Several simulations where conducted to show the gyro system response over a variety of emulated conditions of real world scenarios.

For example Figure 16 shows the system response to a scenario where the bicycle is initially at rest but at an initial offset angle of 20°, which would make the symbolic initial conditions of the system: $\theta_i = 20°$, $\dot{\theta}_i = 0\ \left[\frac{rad}{s}\right]$, $\ddot{\theta}_i = 0\ [\frac{rad}{s^2}]$. At time, t=0, the simulation begins and the gyro's gimbal is instantly actuated by the PID controller to stabilize the system. The plots show that the bicycle is stabilized and returned to $\theta \cong 0°$ within 1 second. Also worth noting is that the gimbal angle, α, also returns to zero as the bicycle angle approaches zero. This condition is desirable because it then puts the gyro system in its optimal position to combat any future disturbances in the bicycle's stability. Each simulation figure shows the plots of the bicycle's angle (θ), the gimbal angle (α), the bicycles angular velocity $(\dot{\theta})$ and acceleration $(\ddot{\theta})$, the torques due to gravity and the gyro acting on the bicycle which are labeled required and reactive torques respectively, and the output signal from the controller which is this simulation is the gimbal angular velocity $(\dot{\alpha})$. In the physical test-bed the gimbal velocity was transformed into a gain proportional to the voltage required to have the gimbal servo motor achieve the desired

motion and velocity. It is also important to note that not only is it crucial that θ approaches zero to stabilize the bicycle, but also that the bicycle's angular velocity and acceleration also approach zero simultaneously which would physically mean that the bicycle would be slowing down as it approached it's semi-stable vertical position and that it did not merely pass through the angle $\theta = 0°$ but that it stopped there. These simulation plots show that this controller stabilizes the bicycle and simultaneously brings it to rest in its balanced position.

Table 3: Values for parameters used in the simulations for stabilization and maneuverability designs. Stabilization simulation parameters are identical to those used in the physical testing of the bicycle.

Mode	Variable / Parameter	Symbol	Value	Unit
Constant	Max Gimbal Rate	$\dot{\alpha}$	5.75	$[rad$
	Rotational spin speed of	Ω	20,000	$[rpm]$
Stabilization	Flywheel mass	m_{fly}	3.33	$[kg]$
	Gyro mass	m_{gyro}	5.55	$[kg]$
	Flywheel Radius	r_g	0.065	$[m]$
	Mass of bicycle	m_{bike}	18.7	$[kg]$
	Center of Gravity, y	h_{bike}	0.27	$[m]$
Maneuverability	Flywheel mass	m_{fly}	30.0	$[kg]$
	Gyro mass	m_{gyro}	50.0	$[kg]$
	Flywheel Radius	r_g	0.195	$[m]$
	Mass of bicycle	m_{bike}	126.3	$[kg]$
	Center of Gravity, x	x_{bike}	0.4914	[m]
	Center of Gravity, y	y_{bike}	0.2465	$[m]$

Simulation results shown in Figure 17 and Figure 19 are tests done to analyze the bicycle's response to greater initial offset angles of $\theta = 60°$ and $\theta = 69°$ respectively with $\dot{\theta}_i = 0\ \left[\frac{rad}{s}\right]$, $\ddot{\theta}_i = 0\ [\frac{rad}{s^2}]$. The simulation shows that from this given model the designed gyro system and flywheel used for all the simulations and the physical model (parameters shown in Table 3) are able to bring the bicycle back to its balanced position.

Although the simulation shows that the gyro can produce enough torque to balance the bicycle from an initial offset angle of $60°$, physical testing will show that the bicycle cannot over a perturbation angle this large with the given flywheel. The sliding mode controller designed by Yetkin was able to more respond faster to the system's non-linearities, thus the SMC was used for the physical test bed control [13]. The 'wake-up' maneuver simulated in Figure 19 attempts to emulate the scenario where the bicycle would be completely on its side, $\theta = 90°$, and bring itself upright. Although the simulations show that the bicycle cannot recover from an initial angle greater than 69°, a flywheel with different parameters (larger radius and mass), with higher operating spin and gimbal speeds would be able to execute this maneuver successfully.

Figure 18 shows the simulation results of a scenario where the bicycle is both initially offset from vertical and has an initial angular velocity (differentiating this simulation from that of Figure 16). The initial conditions for this simulation are symbolically represented by: $\theta_i = 20°$, $\dot{\theta}_i = 1\ \left[\frac{rad}{s}\right]$ $\ddot{\theta}_i = 0\ [\frac{rad}{s^2}]$. The response of this simulation is very similar to that of Figure 16, where the gyro is able to stabilize the system within 1 second, but in this case the gimbal angle is not able to return to zero as the bicycle angle returns to the vertical, $\theta = 0$. Because the gimbal angle, α, comes within 10°, the gyro can simply gimbal the flywheel back to its optimal 0° position at a very slow gimbal rate that would essentially create a negligible amount of reactive torque and therefore the friction in the tires and system would be able to overcome this very minor torque. The flywheel reactive torque Eqn. 10 shows that the reactive torque is linearly related to the gimbal speed, $\dot{\alpha}$, therefore the a very small gimbal speed would produce a very small torque which validates the effectiveness of this approach to solve the problem of non-zero gimbal angle stabilizations. This technique however assumes

that there would not be a large disturbance immediately following the initial disturbance occurring before the gyro were able to slowly gimbal back to its zero angle.

In the dynamic scenario where the bicycle may be traveling forward the bicycle's desired angular orientation would be the same as a static bicycle with $\theta = 0°$. However, if the bicycle were turning a lean would have to be generated and maintained by the gyro without having the flywheel's torque oppose the lean in this scenario but rather hold a specified angle $\theta \neq 0°$. In this case the gyro system input would be given instructions that a turn should be induced and therefore the gyro would execute the maneuver of holding the bicycle at a set desired lean angle for the duration of the turn. In Figure 20 this scenario is simulated and the PID controller is given the target angle of lean to be $10°$. The simulation shows that this gyro design can hold the bicycle at a lean of $\theta \approx 10°$ for just under 1.5 seconds before the gyro could no longer support torque due to gravity acting on the bicycle. This is because as the gyro gimbals, the component of reactive torque acting about the axis that will stabilize the bicycle decreases as explained earlier until. Therefore it can be seen in Figure 20 that as α approached 90° the bicycle was held at its target lean angle but when $\alpha = 90° \rightarrow \cos\alpha = 0 \rightarrow \tau_{gyro} = 0$ which caused the bicycle to fall over.

In the final simulation conducted the bicycle began at an initially stable vertical position and was later introduced by input disturbances. These disturbances took the form of an applied external force acting at a distance (r) from the pivot of rotation of the bicycle which is the axis made by the line created by the bicycle's two tires contact points with the ground. This force acting at a distance from the bicycle's pivot of rotation is essentially a torque, which subsequently causes an angular acceleration due to both the external force and the force due to gravity acting at the bicycles center of mass. The

equation for the relationship between disturbance input force and the resultant angular acceleration is as follows,

[Disturbance Force Input]

$$I\ddot{\theta} = \sum T_x$$

$$I\ddot{\theta} = F * r$$

$$\ddot{\theta} = \frac{F*r}{I} = \frac{F*r}{\frac{1}{2}m_{bike}h_{bike}^2} \quad \left[\frac{rad}{s^2}\right] \tag{20}$$

Figure 21 shows the response of the controller and the system to the two disturbances introduced into the system as force impulses or (input pulse signals) lasting 0.3 seconds each. The first impulse introduced in this simulation is at t=0.5 seconds and then the second impulse is added at t=1.5 seconds. The magnitude of the angular acceleration due to the disturbance force is 4 $\left[\frac{rad}{s^2}\right]$ in the first impulse and -7.5 $\left[\frac{rad}{s^2}\right]$ in the second impulse. As seen in the plots of Figure 21 the controller is able to generate a gyro response that counteracts the impulse disturbance forces and stabilizes the bicycle within one second of the second impulse disturbance (t=2.5 seconds). These impulses, using the above relationship, correspond to around 3-5 N-m or applied external torque that is counteracted by the gyro.

Furthermore, if the PID controller's output signal (currently $\dot{\alpha}$) were to be converted into the voltage signal that it would be in a physical system the following set of equations could be used as a preliminary derivation of the required voltage to provide to the gimbal servo motor to produce the required gimbal behavior. Using the servo motors internal controller an input of the gimbal angle (α) profile with respect to time could also work in executing the required gimbal behavior.

[Gimbal Motor Torque]

$$T_{motor} = I_{flywheel}\ddot{\alpha}$$

$$T_{motor} = (\frac{1}{4}m_{fly}r_{fly}^2 + \frac{1}{12}m_{fly} * t^2)\ddot{\alpha} \quad (21)$$

[Gimbal Motor Voltage and Current Control]

$$V = E_b = K_a\phi\dot{\alpha}$$

$$T_{motor} = K_T\phi I_a$$

3.3 **Physical Test-bed Results**

Once the physical bicycle prototype was equipped with the flywheel, gimbal hardware, mechanical components, sensors, electronics, and micro controllers the bicycle was ready to be tested and the results would then be compared to the results of the simulations. The bicycle setup was controlled via a sliding mode controller designed by two graduate students in the Ohio State University's CITR lab. The controller utilized an accelerometer and IMU to provide the feedback data that was used in the simulation ($\theta, \dot{\theta}, and\ \ddot{\theta}$). The SMC proved to be very robust and performed better in simulations than the simpler PID controller developed in this thesis in terms of minimizing overshoot, decreasing response and settling and rising times. Although the simulations proved greater gyro capabilities the physical experiments did not result in responses as good as those in the simulations. These differences between the simulations and physical tests can be accounted for by the fact that the PID controller in the simulations did not limit the angular acceleration of the gimbal. Therefore, the PID controller generated responses that the servo actuator could not reproduce. Also, the maximum gimbal rate was assumed to be 5.75 rad/s which was also not capable of being reached in the physical testing. The gimbal rate maxed out at around 3.25 rad/s on the physical tests. Finally, the simulations ran the flywheel at a speed of 20,000 rpm whereas the physical test only spun the flywheel at a rate of 12,000 rpm. These factors account for the difference in performance from the simulations to the actual physical testing.

The bicycle was tested starting at initial offset angles at rest (i.e. $\theta = \theta_i$ and $\dot{\theta} = 0$) for initial theta angles ranging between 5° and 20°. The sliding mode controller (SMC) and designed gyro system (same parameters as in the previous section's simulations) was able to stabilize the bicycle for initial theta angles up to $20°$ [13].

The SMC was also responsive to disturbances introduced into the system by applying an external force (or torque) to the bicycles chassis. A different experiment was conducted on the bicycle that used a 0.88 kg mass set to free fall for a period of 2.5 seconds before the weight would be decoupled from the system to end the external impulse. The geometry of the experimental tested set up yielded an applied horizontal force of 6.1 [N] on the bicycle, which resulted in an impulse of 15.26 $\left[kg\,\frac{m}{s^2}\right]$ for 2.5 seconds. The SMC and gyro system were able to overcome this disturbance and stabilize the bicycle. Several other tests of slightly increased weight and reduced

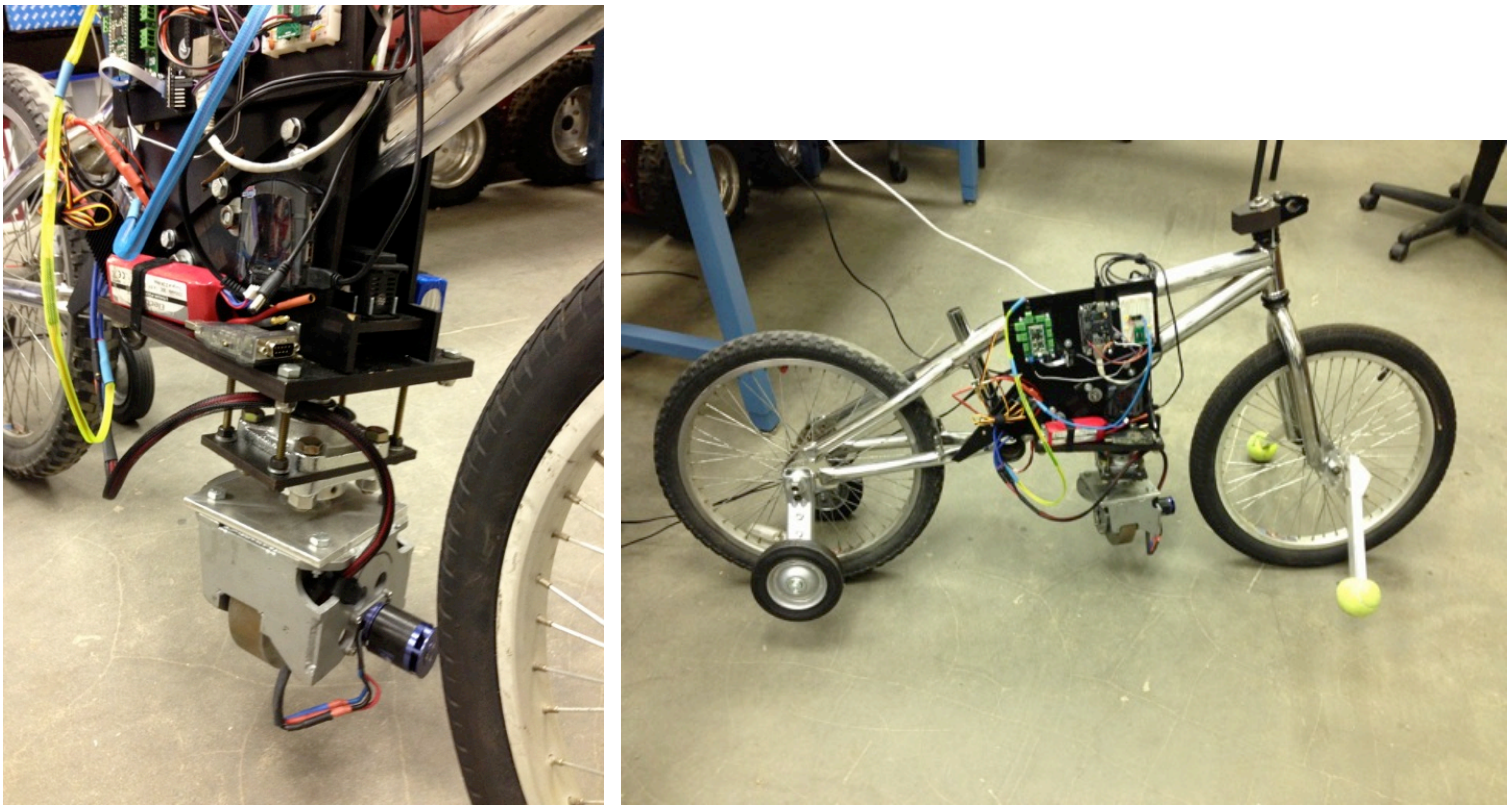

Figure 22: Physical prototype bicycle setup equipped with flywheel, gyro gimballing mechanism, mechanical components, electrical components, and sensors. The bicycle was experimentally tested as shown in this image.

impulse times were also conducted. The results to those experiments can be found in the Yetkin's thesis [13].

4 Bicycle Prototype Platform: Maneuverability

4.1 Dual CMG Design

As mentioned previously, by simply reorienting the gyroscope relative to the bicycle's frame, the CMG can apply its reaction torque about the z-axis, which will instead act to lift the front tire of the bicycle off the ground rather than balance the bicycle laterally about the x-axis. The dynamics of this maneuver will be modeled and simulated to validate the use of a control moment gyroscope to induce a variety of advanced maneuvers on robots and vehicles.

In the design for a single-axis CMG used to balance the bicycle a single gyro was sufficient in creating enough reactive torque to counteract the torque due to gravity and impulses from small disturbances. The torque requirements to lift the front tire of the bicycle off the ground, however, is roughly 1 order of magnitude larger than the required torque for balancing, therefore two counter-rotating flywheels were used in the maneuverability design. Using two gyros for balancing would enable for faster responses and correction to larger disturbances and initial perturbation angles. The use of 2 counter rotating gyros has two positive effects on the control dynamics of the bicycle. It first, doubles the amount of reactive torque able to be produced, which enhances the capabilities of the CMG system in both balancing and maneuverability. The effect of the counter rotation of the flywheels cancels out the component of reaction torque that acts about the undesired axis of rotation once the gyros are gimbaled. This is especially important in the maneuverability design because once the front wheel is lifted off the ground even a relatively small component of unwanted reaction torque about the x-axis

would alter the orientation of the bicycle. This effect can be neglected for balancing because the torque required to lift the bike is much greater and therefore the component of reaction torque acting about the z-axis with one gyro is not sufficient to lift or rotate the bicycle.

A simplified model similar to that for balancing will be derived for the governing equation of motion for inducing wheelie maneuvers. The equation is derived by taking the summation of moments about the z-axis. Again, only two torque (moments) act about the z-axis: the torque due to gravity and the torque due to the two counter rotating flywheels. The equation is derived as follows

$$I_{bike}\ddot{\beta} = \sum M_z = \tau_{gyro,1_z} + \tau_{gyro,2_z} - \tau_{gravity_z} \tag{22}$$

where,

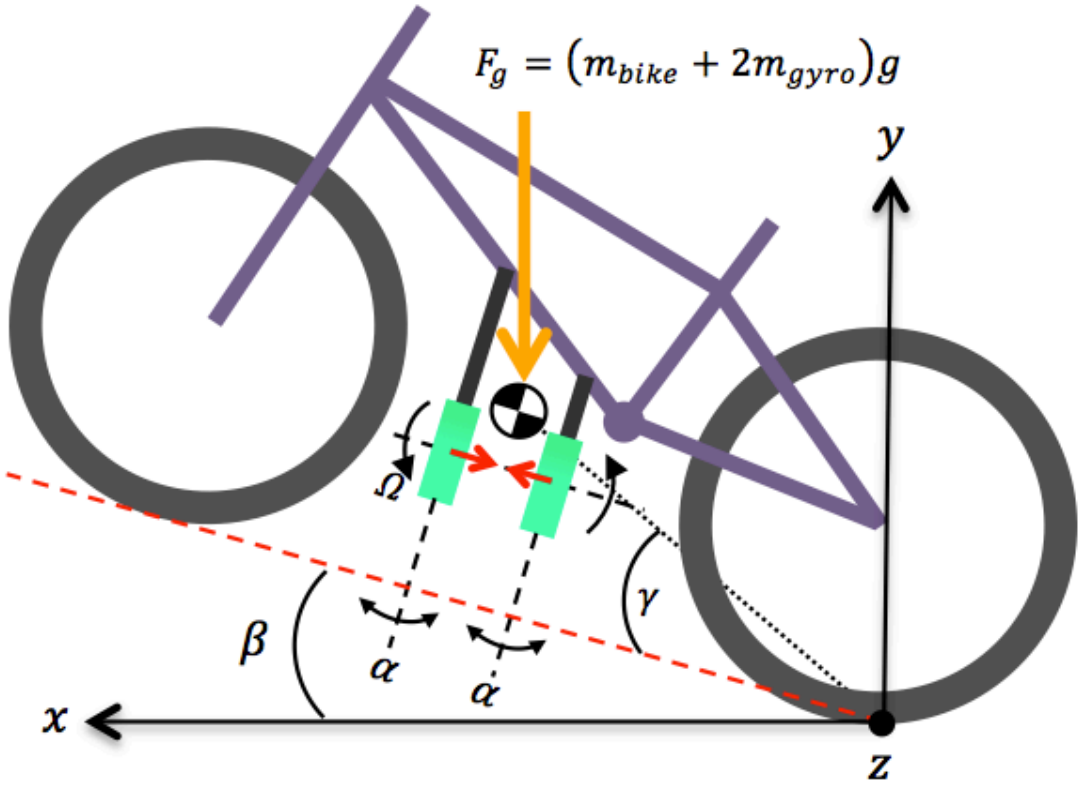

Figure 23: Free body diagram of the bicycle using the 2 counter rotating single-axis gimbal CMG's to perform a 'wheelie'. The flywheels respective angular momentum vectors are shown by the red arrows. The 'wheelie' angle is denoted by $\boldsymbol{\beta}$.

$$\tau_{gyro} = \frac{1}{2}\Omega\ \dot{\alpha}\ \left(m_{fly}\right)\left(r_g^2\right)\left[\cos\alpha\ \hat{k} \pm \sin\alpha\ \ \hat{\imath}\right]$$

$$\tau_{gravity} = m_{bike}(d_{bike})g\cos(\gamma + \beta)$$

$$I_{bike}\ddot{\beta} = \frac{1}{2}\Omega\ \dot{\alpha}\ \left(m_{fly}\right)\left(r_g^2\right)\left[\cos\alpha\ \hat{k} + \sin\alpha\ \ \hat{\imath}\right] + \frac{1}{2}\Omega\ \dot{\alpha}\ \left(m_{fly}\right)\left(r_g^2\right)\left[\cos\alpha\ \hat{k} - \sin\alpha\ \ \hat{\imath}\right] - m_{bike}(d_{bike})g\cos(\gamma + \beta)$$

$$I_{bike}\ddot{\beta} = \Omega\ \dot{\alpha}\ \left(m_{fly}\right)\left(r_g^2\right)\left[\cos\alpha\ \hat{k}\right] - m_{bike}(d_{bike})g\cos(\gamma + \beta) \quad (23)$$

where,

$$d_{bike} = \sqrt{x_{bike}^2 + y_{bike}^2}$$

$$\gamma = \tan^{-1}\frac{y_{bike}}{x_{bike}} = constant$$

In terms of actuating the two single axis gimbal CMGs there are several options that each have their own advantages. The CMGs can be actuated separately via two servo motors. This would allow for faster gimbal rates, which consequently increase the rate of change of angular momentum and thus generate a larger reactive torque. Separate actuation also allows for more advanced control where one gyro can be used to induce a maneuver and the other can be used to balance the bicycle. A simpler actuation method using only one servo motor would be to couple the two gimbals via gear set that counter gimbals the flywheels. This method simplifies the control by only requiring the control and powering of one gimbal motor rather than two but it limits the robustness of the system and the capabilities of the CMGs.

A dual single-axis CMG system was designed but not fabricated or tested for this thesis. Future work on this test bed will aim to validate the maneuverability of CMG systems in physical testing in addition to the simulations conducted in this thesis.

4.2 Maneuverability Dynamics and Simulation

Using the governing equation of motion derived in section 4.1, a Simulink model was created to model the system response of the bicycle configured with 2 single axis gimbal CMGs oriented as shown in Figure 23. With the flywheel parameters listed in Table 3 the 2 CMGs were not capable of producing enough reaction torque to lift the front wheel of the bicycle up and perform and advanced 'wheelie' maneuver. To increase the reactive torque of the CMG system several parameters can be redesigned or changed. Considering that the flywheel mass is dependent on the flywheels radius, width, and material density by,

$$m_{fly} = 2\pi r_g^2 w\rho$$

the most effective method of increasing reaction torque would be to increase the flywheel's radius because this term has an exponential relation to the reaction torque as

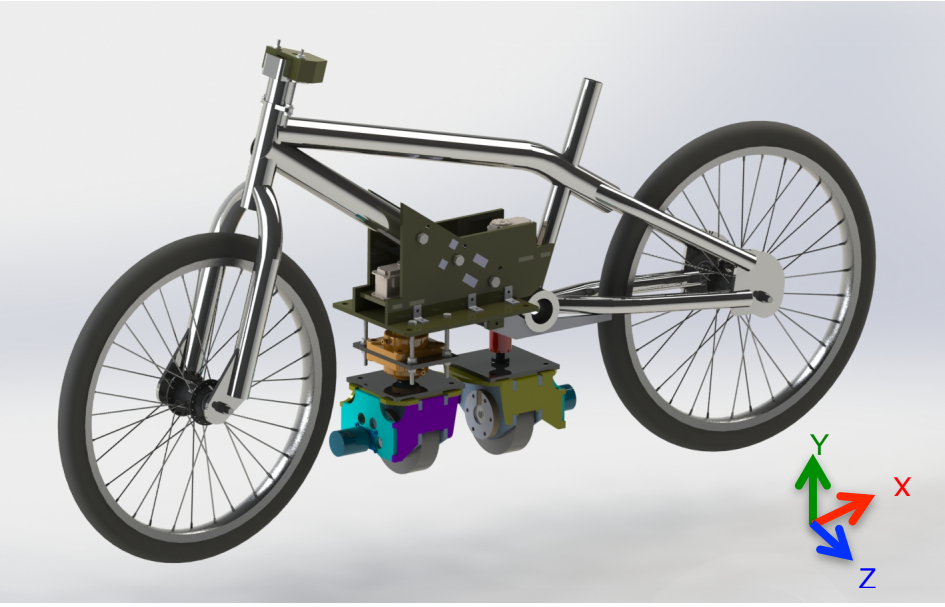

Figure 24: Maneuverability design which incorporates two separately actuated single-axis gimbal counter rotating CMGs.

shown in equation 23. Other methods of increasing the reaction torque of the system include using a stronger flywheel spin or gimbal motor, which would increase Ω and $\dot{\alpha}$ respectively. The flywheels could also be moved towards the rear tire of the bicycle,

which would decrease the moment arm of the gravity force from the pivot of rotation for a wheelie. This would reduce the torque required to rotate the bicycle about its z-axis pivot and perform a wheelie. Due to physical constraints of the design space a larger flywheel cannot be used on the experimental flywheel in its current design, therefore other parameters would have to be adjusted to allow this test bicycle to lift its front wheel off the ground.

Redesigning the bicycle hardware and CMG mounting to allow for a flywheel with radius 0.13 meters (double the original radius) enables the bicycle and dual CMG system to induce the wheelie maneuver and hold positions between $\beta = 0° - 20°$ for nearly 2 seconds. As the flywheel radius is increased the CMG system becomes much more capable in inducing advanced maneuvers and holding wheelie positions of small (most demanding) and large β angles. Therefore, with the reaction torque's high dependency on flywheel radius considered, developing a gyro system for a larger vehicle would be much more feasible because the radius of the flywheel could be 3 times larger (9 times more reaction torque) while only increasing mass by less than 2 times (2 times more required torque). Therefore because required torque would only increase 2 times for the reaction torque's increase of 9 times when scaling up vehicle size, it is clear that inducing advanced maneuvers would be much more feasible on larger vehicles. A simulation was conducted on a vehicle with 2 times as much mass as the original bicycle system and with a flywheel 3 times as large. The parameters of this system are shown in Table 3. As shown in Figure 25 the redesigned vehicle was capable of inducing wheelies with β angles up from 0 to 90 degrees.

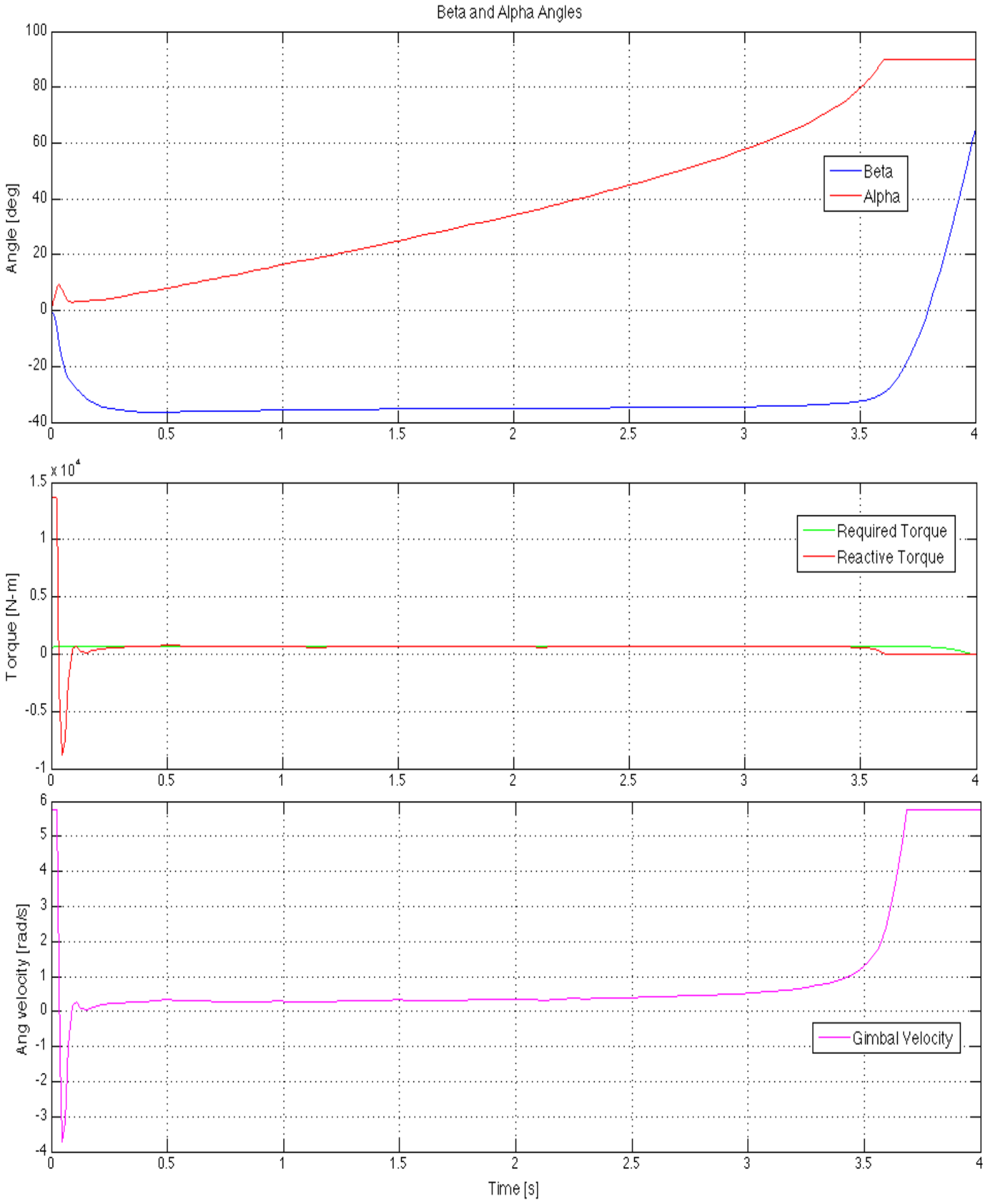

Figure 25: Larger dual flywheel system inducing wheelies of $\boldsymbol{\beta} = \mathbf{35}°$ and maintain the wheelie position for 3.5 seconds. The smaller the desired hold wheelie angle ($\boldsymbol{\beta}$) is, the larger the required torque is. Therefore, the amount of time the flywheels can support holding the wheelie will decrease as $\boldsymbol{\beta}$ decreases to zero.

5 Conclusion

This thesis presents the results of a dynamic analysis and design optimization of a control moment gyroscope system mounted to a bicycle to validate CMG stabilization and advanced maneuverability of inherently unstable vehicles and mobile robots. The physics of gyroscope motion and the mechanical advantage that can be harnessed by gimballing a high-speed flywheel was discussed in section 2. The governing equations of motion for the 3 DOF bicycle system were derived using the Lagrangian. A simplified governing equation was derived with the assumptions that the flywheel gimbal rate was an input from the designed PID controller, the servo motor could accelerate to its max angular velocity instantly, and that the effects of the passive gyro dynamics can be ignored. These assumptions generated a simpler 2^{nd} order ODE used to generate estimates of the system response.

The design of a gimballing mechanism, gyro, mounting hardware, and the optimization of the flywheel geometry were discussed in section 3. Several simulations were conducted for a variety of initial conditions and added disturbances to determine the system response for the stabilization of the bicycle. A physical single-axis gimbal CMG was fabricated and mounted to a bicycle and equipped with motors and controllers. Using a sliding mode controller, as opposed to the PID controller designed in this thesis, the CMG was tested and successfully stabilized the bicycle from the input of several disturbances for an indefinite amount of time. Maneuverability tests were not conducted as it was determined from the simulations that the dual CMG system with the current flywheel geometries would not produce enough reactive torque to lift the front wheel of the bicycle and perform a wheelie. Simulations proved that by scaling up the vehicle size, the flywheel's radius could increase which would significantly increase the amount of

produced reaction torque. Therefore, the simulations also validated the effectiveness of a dual CMG system for larger vehicles in inducing wheelies and advanced maneuvers.

The results of the simulations and experimental bicycle tests validate that an optimized single-axis gimbal CMG can stabilize an inherently unstable mobile robot or in this case of the AFRL project, the Special Ops Vehicle. The results of the maneuverability simulations indicate that with small-scale vehicles it is difficult to induce wheelie maneuvers because the vehicle's design space limits the gyro's flywheel radius. However, for larger vehicles as is the case for the actual prototype AFRL vehicle, the flywheels can be near 3 to 4 times larger. This thesis validates that with a flywheel 3 times larger advanced maneuverability is feasible. A vehicle capable of inducing wheelies while self-balancing would be a significant improvement upon currently existing off-road vehicles.

Future studies may involve the analysis of gyroscopic stabilization of dynamic (i.e. moving) vehicles in either linear driving or turning motions. A more robust and capable CMG design would involve multiple axis gimbals which would give the control system the ability to simultaneously gimbal the gyros to stabilize the vehicle as well as induce advanced maneuvers. With only one, single-axis gimbal gyro, the vehicle can use the CMG to either stabilize the vehicle or to induce a wheelie but not both simultaneously. This is the major limitation of a single axis gimbal gyro. Multiple single-axis gimbal gyros can be used to accomplish multi-objective operation (i.e. balancing and maneuvering).

By continuing the development of CMG stabilization and maneuverability of inherently unstable vehicles and mobile robots, these platforms will be much more robust in traversing rugged real-world environments better than all currently existing technologies. In addition to the AFRL Special Ops vehicle, this technology can be applied to search and rescue robots, extra-terrestrial rovers, field robots, and future personal transportation vehicles to revolutionize the mobility of robotic vehicles.

6 References

[1] Beyer, Steve, Nelson, Philip. “Special Ops Transport Challenge.” Solicitation Number: RFI-PKD-FY11-001. Department of the Air Force, Air Force Material Command. July 20, 2011.

[2] "Gyrocar." *Wikipedia*. Wikimedia Foundation, 15 Feb. 2014. Web. 16 Feb. 2014.

[3] "Gyro Monorail." *Wikipedia*. Wikimedia Foundation, 02 Nov. 2014. Web. 16 Feb. 2014.

[4] Doppelbauer, Martin. "A short history of electric motors, 1800-1893". Karlsruhe Institute of Technology.

[5] "Electric Motor." *Wikipedia*. Wikimedia Foundation, 14 Feb. 2014. Web. 14 Feb. 2014.

[6] Lavrinc, Damon (2012-05-29). "Exclusive: This Is the Gyro-Stabilized, Two-Wheeled Future of Transportation | Autopia". Wired.com.

[7] J. P. Meijaard, J. M. Papadopoulos, A. Ruina, and A. L. Schwab (2007). "Linearized dynamics equations for the balance and steer of a bicycle: a benchmark and review" (PDF). *Proceedings of the Royal Society A* **463** (2084): 1955–1982. Bibcode:2007RSPSA.463.1955M. doi:10.1098/rspa.2007.1857.

[8] "Control Moment Gyroscope." *Wikipedia*. Wikimedia Foundation, 15 Feb. 2014. Web. 16 Feb. 2014.

[9] Lewin, Walter. "Gyroscope Physics." *Gyroscope Physics*. N.p., 2 Dec. 2012. Web. 20 Dec. 2013.

[10] Meriam, J.L. and Kraige L.G.. *Engineering Mechanics: Dynamics*. 2nd Edition. New York: John Wiley & Sons, Inc., 1986.

[11] "Lec 24 | 8.01 Physics I: Classical Mechanics, Fall 1999." *YouTube*. YouTube, 14 Jan. 2008. Web. 20 Dec. 2013.

[12] "Solving the Mystery of Gyroscopes." *YouTube*. YouTube, 28 Mar. 2012. Web. 20 Dec. 2013.

[13] Yetkin, Harun. “Stabilization of Autonomous Bicycle.” Masters Thesis, The Department of Electrical and Computer Engineering, The Ohio State University, 2013.

[14] Zinober, A.S.I., ed. (1990). *Deterministic control of uncertain systems*. London: Peter Peregrinus Press. ISBN 978-0-86341-170-0.

[15] "Engineering Materials." *Engineering Materials*. N.p., n.d. Web. 16 Feb. 2014.

[16] Collins, J. A. *Mechanical Design of Machine Elements and Machines: A Failure Prevention Perspective*. New York, NY: Wiley, 2003. Print.

[17] Shelquist, Richard. "Equations - Air Density and Density Altitude." *Equations - Air Density and Density Altitude*. N.p., 2 Dec. 2012. Web. 27 Dec. 2013.

[18] Beardmore, Roy. "Rolling Bearing Friction." *Rolling Bearing Friction*. N.p., 9 Sept. 2011. Web. 20 Dec. 2013.

[19] Genta, Giancarlo (1985). *Kinetic Energy Storage*. London: Butterworth & Co. Ltd.

[20] Richardson, K. I. T. *The Gyroscope Applied.* London: Hutchinson's Scientific and Technical Publications, 1954. Print.

APPENDIX A

Derivation of Governing ODE's for The Motion of a Gyro on a Hinge

There are 2 degrees of freedom, θ and α. Treating the gyro as a thin plate, we will derive two coupled 2nd order O.D.E's for θ and α. We will use a brute force langrangian approach.

$$L(\theta, \alpha) = \mathrm{T} - \mathrm{V}$$

Where:

$$\mathrm{T} = kinetic = \frac{1}{2} I_{bike} \dot{\theta}^2 + \frac{1}{2} \int_{GYRO} dm \left(\dot{\vec{x}}_{GYRO}\right)^2$$

$$\mathrm{V} = \text{gravitational potential} = \left((\mathrm{M_{BIKE}})(g)\left(h_{BIKE_{CG}}\right) + M_{GYRO} * R \right) \cos\theta = \mathrm{V_o}$$

Euler-Lagrange Equations:

$$\frac{\partial \mathrm{L}}{\partial \theta} = \frac{d}{dt}\left(\frac{\partial \mathrm{L}}{\partial \dot{\theta}}\right)$$
$$\frac{\partial \mathrm{L}}{\partial \alpha} = \frac{d}{dt}\left(\frac{\partial \mathrm{L}}{\partial \dot{\alpha}}\right)$$

These will give us our two ODE's.

The only hang up is that we need to explicitly compute the kinetic energy of the gyro, $\frac{1}{2}\int dm\left(\dot{\vec{x}}_{GYRO}\right)^2$, as a function of α and θ. Once we do that, we will have an explicit function (the Lagrangian), L(θ,α) from which we can get the equations of motion.

To initiate this integral define a coordinate system $\hat{e}_1, \hat{e}_2, \hat{e}_3$, that is fixed to the gyro and which rotates along with it. Every chunk of the gyro is nicely coordinated in this basis. Note that in general $\hat{e}_1, \hat{e}_2, \hat{e}_3$ will point in random directions with respect to $\hat{x}, \hat{y}, \hat{z}$.

$$\vec{x}_{GYRO} = \vec{R} + u\cos\phi\ \hat{e}_1 + u\sin\phi\ \hat{e}_2$$

Note that u and ϕ are time independent coordinates that permit $\int dm\left(\dot{\vec{x}}_{GYRO}\right)^2$ to be written as $\int_0^{r_G}\int_0^{2\pi}\mu * u\, du\, d\theta\, \left(\dot{\vec{x}}_{GYRO}\right)^2$ where μ is the (surface) mass density of the gyro and r_G is its radius.

$$\left(\dot{\vec{x}}_{GYRO}\right)^2 = (\dot{\vec{R}} + u\cos\phi\,\dot{\hat{e}}_1 + u\sin\phi\,\dot{\hat{e}}_2)^2$$

$$= \left(\dot{\vec{R}}\right)^2 + (u\cos\phi\,\dot{\hat{e}}_1 + u\sin\phi\,\dot{\hat{e}}_2)^2 + 2\dot{\vec{R}} * (u\cos\phi\,\dot{\hat{e}}_1 + u\sin\phi\,\dot{\hat{e}}_2)$$

$$= R^2\left(\dot{\hat{R}}\right)^2 + u^2\cos^2\phi\left(\dot{\hat{e}}_1\right)^2 + u^2\sin^2\phi\left(\dot{\hat{e}}_2\right)^2 + 2u\sin\phi\cos\phi\left(\dot{\hat{e}}_1\right)\left(\dot{\hat{e}}_2\right) + 2uR(\cos\phi\,\dot{\hat{R}} * \dot{\hat{e}}_1 + \sin\phi\,\dot{\hat{R}} * \dot{\hat{e}}_2)$$

$$\therefore\ \ \frac{1}{2}\mu\int_0^{r_g} du\ \int_0^{2\pi} d\theta\ \ u\left(\dot{\vec{x}}_{GYRO}\right)^2 = \frac{1}{2}\mu\left[R^2\left(\dot{\hat{R}}\right)^2\pi r_g^2 + \frac{\pi r_g^4}{4}\left(\dot{\hat{e}}_1\right)^2 + \frac{\pi {r_g}^4}{4}\left(\dot{\hat{e}}_2\right)^2 + 0 + 0\right]$$

***note: $\hat{e}_1, \hat{e}_2$ are turning and twisting around so they are time dependent unlike $\hat{x}, \hat{y}, \hat{z}$.

$$\mathrm{T_{GYRO}} = R^2\left(\dot{\hat{R}}\right)^2 * \frac{1}{2}M_{GYRO} + \frac{r_g^2}{8}M_{GYRO}\left(\left(\dot{\hat{e}}_1\right)^2 + \left(\dot{\hat{e}}_2\right)^2\right)$$

Recall that we need to get this as an explicit function of θ and α (and constants)

1) $\dot{\hat{R}} = ?$ "α, θ"

$\hat{R} = \sin\theta\hat{x} + cos\theta\hat{y}$

$\dot{\hat{R}} = \dot{\theta}\cos\theta\hat{x} - \dot{\theta}sin\theta\hat{y}$

$\left(\dot{\hat{R}}\right)^2 = \dot{\theta}^2(\cos^2\theta + \sin^2\theta) = \dot{\theta}^2$

2) $\left(\dot{\hat{e}}_1\right)^2 + \left(\dot{\hat{e}}_2\right)^2 = ?$ "α, θ"

This one will get messy considering we need to relate $\hat{e}_1, \hat{e}_2, \hat{e}_3$ to the lab frame. The gyro rotates in the (moving) $\hat{R}, \hat{R}\times\hat{\Omega}$ plane. Then $\hat{e}_1$ and $\hat{e}_2$ can be related to $\hat{R}$ and $\hat{\Omega}$ via the following:

$$\begin{pmatrix}\hat{e}_1\\ \hat{e}_2\end{pmatrix} = \begin{pmatrix}\cos\Omega t & \sin\Omega t\\ -\sin\Omega t & \cos\Omega t\end{pmatrix}\begin{pmatrix}\hat{R}\times\hat{\Omega}\\ \hat{R}\end{pmatrix}$$

which may be confirmed by showing that $\hat{e}_1 * \left(\hat{R}\times\hat{\Omega}\right) = \cos\Omega t$ etc. From this point $\hat{R}$ and $\hat{\Omega}$ can be expressed in terms of $\hat{x}, \hat{y}, \hat{z}$, as was done in the first iteration solution of this problem. Explicitly, for later reference:

$$\hat{R} = \sin\theta\hat{x} + \cos\theta\hat{y}$$

$$\hat{\Omega} = -\cos\alpha\cos\theta\,\hat{x} + \cos\alpha sin\theta\,\hat{y} + sin\alpha\,\hat{z}$$

Now, to solve the above system of equations using linear algebra techniques,

$$\left(\dot{\hat{e}}_1\right)^2 + \left(\dot{\hat{e}}_2\right)^2 = \begin{pmatrix}\dot{\hat{e}}_1 & \dot{\hat{e}}_2\end{pmatrix}\begin{pmatrix}\dot{\hat{e}}_1\\ \dot{\hat{e}}_2\end{pmatrix} \equiv \dot{x}^T\dot{x}$$

Let $\quad x = O * y; \qquad x \equiv \begin{pmatrix}\hat{e}_1\\ \hat{e}_2\end{pmatrix}; \qquad y \equiv \begin{pmatrix}\hat{R}\times\hat{\Omega}\\ \hat{R}\end{pmatrix}; \qquad \begin{pmatrix}\cos\Omega t & \sin\Omega t\\ -\sin\Omega t & \cos\Omega t\end{pmatrix} = 0$

$$\begin{aligned}\dot{x}^T\dot{x} &= \left[\frac{d}{dt}(O*y)\right]^T\left[\frac{d}{dt}(O*y)\right]\\ &= \left[\dot{O}y + O\dot{y}\right]^T\left[\dot{O}y + O\dot{y}\right]\\ &= \left[(\dot{y})^T O^T + \dot{y}^T\left(\dot{O}\right)^T\right]^T\left[Oy^{\cdot} + O\dot{y}\right]\\ &= (\dot{y})^T O^T O^{\cdot} y + y^T\left(\dot{O}\right)^T O\dot{y} + (\dot{y})^T O^T O\dot{y} + y^T\left(\dot{O}\right)^T\dot{O}y\\ &= 2y^T\left(\dot{O}\right)^T O\dot{y} + (\dot{y})^T\dot{y} + y^T\Omega^2 y\end{aligned}$$

where in this last step we have used several equating properties:

$$(\dot{y})^T O^T\dot{O}y = \left((\dot{y})^T O^T\dot{O}y\right)^T = y^T\left(\dot{O}\right)^T O(\dot{y})$$

This makes sense because the whole term is a scalar and the transpose of a scalar is itself. Also, we have used the fact that $O^T O = Identity\ Matrix$, since O is an orthogonal (rotation) matrix.

$$\left(\dot{O}\right)^T\dot{O} = \begin{pmatrix}-\Omega\sin\Omega t & \Omega\cos\Omega t\\ -\Omega\cos\Omega t & -\Omega\sin\Omega t\end{pmatrix}^T\begin{pmatrix}-\Omega sin & \Omega cos\\ -\Omega cos & -\Omega sin\end{pmatrix} = \Omega^2\begin{pmatrix}1 & 0\\ 0 & 1\end{pmatrix}$$

$$\left(\dot{\hat{e}}_1\right)^2 + \left(\dot{\hat{e}}_2\right)^2 = 2y^T\left(\dot{O}\right)^T O\dot{y} + (\dot{y})^T\dot{y} + y^T\Omega^2 y$$

$$\left(\dot{O}\right)^T O = \begin{pmatrix} -\Omega\sin\Omega t & \Omega\cos\Omega t \\ -\Omega\cos\Omega t & -\Omega\sin\Omega t \end{pmatrix}^T \begin{pmatrix} cos & sin \\ -sin & cos \end{pmatrix} = -\Omega\begin{pmatrix} s & c \\ -c & s \end{pmatrix}\begin{pmatrix} c & s \\ -s & c \end{pmatrix}$$

$$= -\Omega\begin{pmatrix} 0 & 1 \\ -1 & 0 \end{pmatrix}$$

Now, because $\left(\hat{R}\times\hat{\Omega}\right)$ and $\hat{R}$ are both unit vectors, the following is true:

$$y^T y = \begin{pmatrix} \hat{R}\times\hat{\Omega} & \hat{R} \end{pmatrix}\begin{pmatrix} \hat{R}\times\hat{\Omega} \\ \hat{R} \end{pmatrix} = \left(\hat{R}\times\hat{\Omega}\right) * \left(\hat{R}\times\hat{\Omega}\right) + \hat{R} * \hat{R} = 2$$

$$(\dot{y})^T\dot{y} = \left[\partial_t\left(\hat{R}\times\hat{\Omega}\right)\right]^2 + \left[\dot{\hat{R}}\right]^2 = \left[\partial_t\left(\hat{R}\times\hat{\Omega}\right)\right]^2 + \dot{\theta}^2$$

$$\left(\dot{\hat{e}}_1\right)^2 + \left(\dot{\hat{e}}_2\right)^2 = -2\Omega\begin{pmatrix} \hat{R}\times\hat{\Omega} & \hat{R} \end{pmatrix}\begin{pmatrix} 0 & 1 \\ -1 & 0 \end{pmatrix}\begin{pmatrix} \partial_t\left(\hat{R}\times\hat{\Omega}\right) \\ \left(\dot{\hat{R}}\right) \end{pmatrix} + \left[\partial_t\left(\hat{R}\times\hat{\Omega}\right)\right]^2 + \dot{\theta}^2 + 2\Omega^2$$

$$= -2\Omega\left(\left(\hat{R}\times\hat{\Omega}\right) * \left(\dot{\hat{R}}\right) - \hat{R}\,\partial_t\left(\hat{R}\times\hat{\Omega}\right)\right) + \left[\partial_t\left(\hat{R}\times\hat{\Omega}\right)\right]^2 + \dot{\theta}^2 + 2\Omega^2$$

$$= -2\Omega\left(\left(\hat{R}\times\hat{\Omega}\right) * \left(\dot{\hat{R}}\right) - \hat{R} * \left(\dot{\hat{R}}\times\hat{\Omega} + \hat{R}\times\dot{\hat{\Omega}}\right)\right) + \left[\partial_t\left(\hat{R}\times\hat{\Omega}\right)\right]^2 + \dot{\theta}^2 + 2\Omega^2$$

Using the vector identities $A\times B = -B\times A$ and $A * (B\times C) = (A\times B) * C$ to rearrange the second term within the larger term that is multiplied by -2Ω we get:

$$= -4\Omega\left(\hat{R}\times\hat{\Omega}\right) * \dot{\hat{R}} + \left[\partial_t\left(\hat{R}\times\hat{\Omega}\right)\right]^2 + \dot{\theta}^2 + 2\Omega^2$$

To get $\hat{R}\ and\ \hat{\Omega}$ in terms of $\theta\ and\ \alpha$,

$$\hat{R}\times\hat{\Omega} = (\sin\theta\,\hat{x} + \cos\theta\,\hat{y})\times(-\cos\alpha\cos\theta\,\hat{x} + \cos\alpha\sin\theta\,\hat{y} + \sin\alpha\,\hat{z})$$

$$= \sin\theta(\cos\alpha\sin\theta\,\hat{z} + \sin\alpha(-\hat{y})) + \cos\theta(\cos\alpha\cos\theta\,\hat{z} + \sin\alpha\,\hat{x})$$

$$= \sin\alpha\cos\theta\,\hat{x} - \sin\alpha\sin\theta\,\hat{y} + \cos\alpha\,\hat{z}$$

$$\therefore \left(\hat{R}\times\hat{\Omega}\right) * \dot{\hat{R}} = (\sin\alpha\cos\theta\,\hat{x} - \sin\alpha\sin\theta\,\hat{y} + \cos\alpha\,\hat{z}) * (\cos\theta\,\hat{x} - \sin\theta\,\hat{y})\dot{\theta}$$

$$\left(\hat{R}\times\hat{\Omega}\right) * \dot{\hat{R}} = \dot{\theta}(\sin\alpha\cos^2\theta + \sin\alpha\sin^2\theta)$$

$$= \dot{\theta}\sin\alpha$$

$$\partial_t\left(\hat{R}\times\hat{\Omega}\right) = (\dot{\alpha}\cos\alpha\cos\theta - \dot{\theta}\sin\alpha\sin\theta)\hat{x} - (\dot{\alpha}\cos\alpha\sin\theta + \dot{\theta}\sin\alpha\cos\theta)\hat{y} - (\dot{\alpha}\sin\alpha)\hat{z}$$

$$\left[\partial_t\left(\hat{R}\times\hat{\Omega}\right)\right]^2 = \dot{\alpha}^2\cos^2\alpha + \dot{\theta}^2\sin^2\alpha + \dot{\alpha}^2\sin^2\alpha$$

$$= \dot{\alpha}^2 + \dot{\theta}^2\sin^2\alpha$$

$$\left(\dot{\hat{e}}_1\right)^2 + \left(\dot{\hat{e}}_2\right)^2 = -4\Omega\dot{\theta}\sin\alpha + \dot{\alpha}^2 + \dot{\theta}^2\sin^2\alpha + \dot{\theta}^2 + 2\Omega^2$$

$$\mathrm{T}_{GYRO} = \frac{1}{2}M_{GYRO}R^2\dot{\theta}^2 + \frac{r_g^2}{8}M_{GYRO}(-4\Omega\dot{\theta}\sin\alpha + \dot{\alpha}^2 + \dot{\theta}^2\sin^2\alpha + \dot{\theta}^2 + 2\Omega^2)$$

$$L(\theta,\alpha) = \frac{1}{2}\left(I_{BIKE}M_{GYRO}R^2 + \frac{1}{4}M_{GYRO}r_g^2(1+\sin^2\alpha)\right)\dot{\theta}^2 + \frac{1}{8}M_{GYRO}r_g^2\dot{\alpha}^2 - \frac{1}{2}M_{GYRO}r_g^2\Omega\dot{\theta}\sin\alpha \ldots$$

$$\ldots + \frac{1}{4}M_{GYRO}r_g^2\Omega^2 - \mathrm{V}_o\cos\theta$$

$$\frac{\partial \mathrm{L}}{\mathrm{d}\theta} = \frac{d}{dt}\left(\frac{\partial \mathrm{L}}{\partial\dot{\theta}}\right)$$

$$\mathrm{V}_o\sin\theta = \frac{d}{dt}\left[\left(I_{BIKE} + M_{GYRO}R^2 + \tfrac{1}{4}M_{GYRO}r_g^2(1+\sin^2\alpha)\right)\dot{\theta} - \tfrac{1}{2}M_{GYRO}r_g^2\Omega\sin\alpha\right]$$

$$\therefore \quad \mathbf{0} = \left(\boldsymbol{I_{BIKE}} + \boldsymbol{M_{GYRO}R^2} + \frac{1}{4}\boldsymbol{M_{GYRO}r_g^2}(\mathbf{1}+\sin^2\boldsymbol{\alpha})\right)\ddot{\boldsymbol{\theta}} + \frac{1}{2}\boldsymbol{M_{GYRO}r_g^2}\dot{\boldsymbol{\alpha}}\dot{\boldsymbol{\theta}}\sin\boldsymbol{\alpha}\cos\boldsymbol{\alpha} \ldots$$

$$\ldots - \frac{1}{2}\boldsymbol{M_{GYRO}r_g^2\Omega}\,\frac{\boldsymbol{d}(\sin\boldsymbol{\alpha})}{\boldsymbol{dt}} - \mathbf{V}_{\boldsymbol{o}}\sin\boldsymbol{\theta}$$

$$\frac{\partial \mathrm{L}}{\partial\alpha} = \frac{d}{dt}\left(\frac{\partial \mathrm{L}}{\partial\dot{\alpha}}\right)$$

$$\tfrac{1}{2}*\tfrac{1}{4}M_{GYRO}r_g^2 * 2\dot{\theta}^2\sin\alpha\cos\alpha - \tfrac{1}{2}M_{GYRO}r_g^2\Omega\dot{\theta}\cos\alpha = \frac{d}{dt}\left[\tfrac{1}{4}\,M_{GYRO}r_g^2\dot{\alpha}\right]$$

$$M_{GYRO}r_g^2\,\dot{\theta}^2\sin\alpha\cos\alpha - 2M_{GYRO}r_g^2\Omega\,\dot{\theta}\cos\alpha - M_{GYRO}r_g^2\ddot{\alpha} = 0$$

$$\therefore \quad \mathbf{0} = \ddot{\boldsymbol{\alpha}} - \boldsymbol{\sin\alpha\cos\alpha}\,\dot{\boldsymbol{\theta}} + \boldsymbol{2\Omega\dot{\theta}\cos\alpha}$$

APPENDIX B

```
% Flywheel Optimization
% Simon Kalouche
% Honors Undergraduate Thesis
% Mechanical Engineering

clear
close all
clc

%Program optimizes the radius of the flywheel and therefore the mass of the
%flywheel for a given initial bike offset angle, flywheel thickness, and
%gimbal rate

%Assumptions: the center of mass of the bicycle with the gyro is assumed to
%not be a function of the radius therefore it is held constant



%r_fly=                          %[m] radius of flywheel
%m_fly=                          %[kg] mass of flywheel
%m_gyro=                         %[kg] estimate for the weight of flywheel
                                 % with housing (i.e. weight of whole gyro)
%m_bike=                         %[kg] mass of bike with gyro hardware

den=7850;                        %[kg/m^3] density of steel flywheel
%den=19250;                      %[kg/m^3] density of tungsten flywheel
t=0.032;                         %[m] thickness of flywheel
h_bike=.27;                      %center of gravity of bike with gyro
theta=20;      %angle bicycle is offset from verticle
w=20000*2*pi()/60;               %[rad/s] ang velocity of flywheel
g=9.81;                          %[m/s^2] gravity
alpha_d=5.75;                    %[rad/s] gimbal angular velocity
I_bike=1.86;                     %[kg-m^2] moment of inertia of bike about rotatic

i=1;
for t=.025:.005:.050
r_fly=.01:.001:.1;
m_fly=pi()*((r_fly).^2)*t*den;
m_gyro=m_fly*2-(1/3)*m_fly;
m_bike=13.14+m_gyro;
t_req=(m_bike+m_gyro)*g*h_bike*sind(theta); %[N-m]
L=(0.5)*(m_fly).*(power(r_fly,2)).*w;  %[kg*m^2/s] angular momentum
t_gyro=L*alpha_d;      %[N-m]


hold on
%subplot(3,2,i)
%plot(r_fly,t_gyro,'b',r_fly,t_req,'r')
plot(r_fly,t_gyro,r_fly,t_req)
if i>=6
title(sprintf('Flywheel Optimization: thickness= 0.025 - %f [m]',t));
xlim([0.01,.1]);
```

```
ylim([0,150]);
xlabel('Flywheel Radius (m)');
ylabel('Torque (N-m)')
legend('Flywheel Reaction Torque','Required Stabilization Torque')
grid on
end

i=i+1;
end

hold on

theta=0:.001:20;
r_fly=.06;
t=.032;
m_fly=pi()*((r_fly).^2)*t*den;
m_gyro=m_fly*2-(1/3)*m_fly;
m_bike=13.14+m_gyro;

ratio=m_fly/m_bike

t_req=(m_bike+m_gyro)*g*h_bike*sind(theta);
L=(0.5)*(m_fly).*(power(r_fly,2)).*w;
t_gyro_max=L*alpha_d




% figure
% alpha_d=(1.1)*t_req/L;
% alpha=-(1.1*(m_bike+m_gyro)*g*h_bike.*cosd(theta)./L);
% t_gyro=L*alpha_d.*cosd(alpha);
% alpha_d=t_gyro/L;

% subplot(2,1,1)
% plot(theta, t_req, theta, t_gyro, theta, alpha_d)
% xlabel('Theta (degrees)');
% %ylabel('Required Torque (N-m)');
% legend('Torque Required', 'Gyro Torque', 'Required Gimbal Speed to Stabilize')
% subplot(2,1,2)
% theta_dd=(t_gyro-t_req)/I_bike;
% plot(theta, theta_dd)


% Design Specs after optimization plots
t_req=(m_bike+m_gyro)*g*h_bike*sind(20)


%This program validates that a flywheel with radius> approx. 6 cm, and
%thickness of 3 cm can stabilize the bicycle with an initial offset angle
%of 20 degrees
```

```
%-------------------------------------------------------------

% Calculate Critical Flywheel Stress

stress_cr=.5*den*(r_fly^2)*(w^2)/(10^6)        %[MPa] Tensile Stress on flywheel


% Calculate torque (loss) due to air resistance


nu=1.983;                          %[kg/m*s] dynamic viscosity of air at 300K
p_air=1.164;                       %[kg/m^3] density of air
Re=p_air*(r_fly^2)*w/nu;           %reynolds number
Cm=3.87*Re^(-.5);                  %air flow type constant

T_air=p_air*(w^2)*(r_fly^5)*Cm


% Calculate torque (loss) due to bearing friction


mu=.0015;                          %coef. of friction for single row ball bearing w/
F_r=m_fly*g;
f_bearing=mu*F_r;
d_bore=.00635;                     %[m] 1/4" diameter bore
T_bearing=f_bearing*d_bore*(1/2)


% Energy to spin flywheel up to speed
E_start=(.25)*m_fly*(r_fly^2)*w^2
```

```
ratio =

    0.1589


t_gyro_max =

   61.5844


t_req =

   20.4826


stress_cr =

   61.9811


T_air =
```

```
    7.3037
```

```
T_bearing =

   1.3273e-04
```

```
E_start =

   1.1216e+04
```

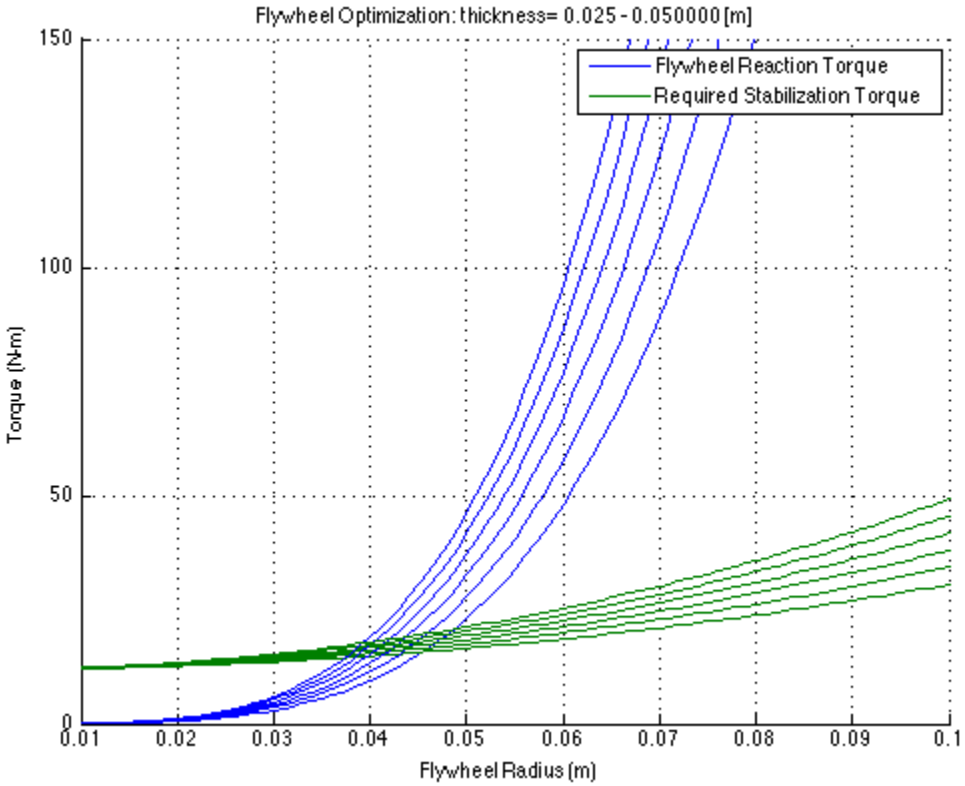

Published with MATLAB® R2013a

```
clear
close all
clc

%Program optimizes the radius of the flywheel and therefore the mass of the
%flywheel for a given initial bike offset angle, flywheel thickness, and
%gimbal rate

%Assumptions: the center of mass of the bicycle with the gyro is assumed to
%not be a function of the radius therefore it is held constant



g=9.81;                          %[m/s^2] gravity
den=7850;                        %[kg/m^3] density of steel flywheel
t=0.032;                         %[m] thickness of flywheel
h_bike=.27;                      %[m] center of gravity of bike with gyro
w=20000*2*pi()/60;               %[rpm] rev per minute of flywheel
I_bike=1.86;                     %[kg/cm^2] bicycle moment of inertia

% initial conditions
theta_i=20*pi()/180;              %[rad] angle bicycle is offset from verticle
theta_d=1;                       %[rad/s] initial bicycle angular velocity

%Step Disturbances
step_time1=.5;                      %[s] when step disturbance is introduced
disturbance1=0;                    %[rad/s] bicycle step distrubance ang velocity

step_time2=1.5;                       %[s] when step disturbance is introduced
disturbance2=0;                     %[rad/s] bicycle step distrubance ang velocit

step_time3=2.25;                    %[s] when step disturbance is introduced
disturbance3=0;                     %[rad/s] bicycle step distrubance ang velocit



%alpha_d=2.0015;                 %[rad/s] gimbal angular velocity
%time=0:.001:3;                  %[s] time in seconds

r_fly=.065;                              %[m] radius of flywheel
m_fly=pi()*((r_fly).^2)*t*den;           %[kg] mass of flywheel
m_gyro=m_fly*2-(1/3)*m_fly;              %[kg] estimate for the weight of flywheel
                                         % with housing (i.e. weight of whole gyro
m_bike=13.14+m_gyro;                     %[kg] mass of bike with gyro hardware
L=(0.5)*(m_fly).*(power(r_fly,2)).*w;    %[kg*m^2/s] angular momentum
alphaDmax=5.75;                          %[rad/s] maximum gimbal velocity
theta_target=0*pi()/180;                %[rad] target theta used as input to contr

%alpha=time*alpha_d;
%t_gyro=L*alpha_d*cos(alpha);      %[N-m]

sim('sumOfTorqueStabilization')
```

```
theta=theta*180/pi();
alpha=alpha*180/pi();

%*********************************************************************
% Individual Plots


plot(time, theta, 'b', time, alpha, 'r')
title(sprintf('Theta and Alpha Angles ( ICs  theta = 20, theta* = 0 )'))
legend('Theta','Alpha')
xlabel('Time [s]');
ylabel('Angle [deg]')
grid on


% figure
% plot(time, t_req, 'g', time, t_reactive, 'r')
% title('Required and Reactive Torques')
% legend('Required Torque','Reactive Torque')
% xlabel('Time [s]');
% ylabel('Torque [N-m]')
% grid on
%
% figure
% plot(time, theta_d, 'k')
% title('Angular Velocity of Bicycle')
% legend('angular velocity')
% xlabel('Time [s]');
% ylabel('Ang Velocity [rad/s]')
% grid on
%
% figure
% plot(time, theta_dd, 'm')
% title('Angular Acceleration of Bicycle')
% legend('angular accel.')
% xlabel('Time [s]');
% ylabel('Ang accel. [rad/s^2]')
% grid on
%
% figure
% plot(time, alphaD_prof, 'm')
% title('Angular Velocity of Gimbal')
% legend('Gimbal Velocity')
% xlabel('Time [s]');
% ylabel('Ang velocity [rad/s]')
% grid on


%*********************************************************************
% All Plots on one figure
```

```
figure
subplot(5,1,1)
plot(time, theta, 'b', time, alpha, 'r')
title('Theta and Alpha Angles')
legend('Theta','Alpha')
xlabel('Time [s]');
ylabel('Angle [deg]')
grid on

subplot(5,1,2)
plot(time, theta_d, 'k')
title('Angular Velocity of Bicycle')
legend('Bicycle angular velocity')
xlabel('Time [s]');
ylabel('Ang Velocity [rad/s]')
grid on

subplot(5,1,3)
plot(time, theta_dd, 'm')
title('Angular Acceleration of Bicycle')
legend('Bicycle angular accel.')
xlabel('Time [s]');
ylabel('Ang accel. [rad/s^2]')
grid on

%figure
subplot(5,1,4)
plot(time, t_req, 'g', time, t_reactive, 'r')
title('Required and Reactive Torques')
legend('Required Torque','Reactive Torque')
xlabel('Time [s]');
ylabel('Torque [N-m]')
grid on


subplot(5,1,5)
plot(time, alphaD_prof, 'm')
title('Angular Velocity of Gimbal')
legend('Gimbal Velocity')
xlabel('Time [s]');
ylabel('Ang velocity [rad/s]')
grid on
```

```
Warning: Using a default value of 0.06 for maximum step size.  The simula
step size will be equal to or less than this value.  You can disable this
diagnostic by setting 'Automatic solver parameter selection' diagnostic t
'none' in the Diagnostics page of the configuration parameters dialog
```

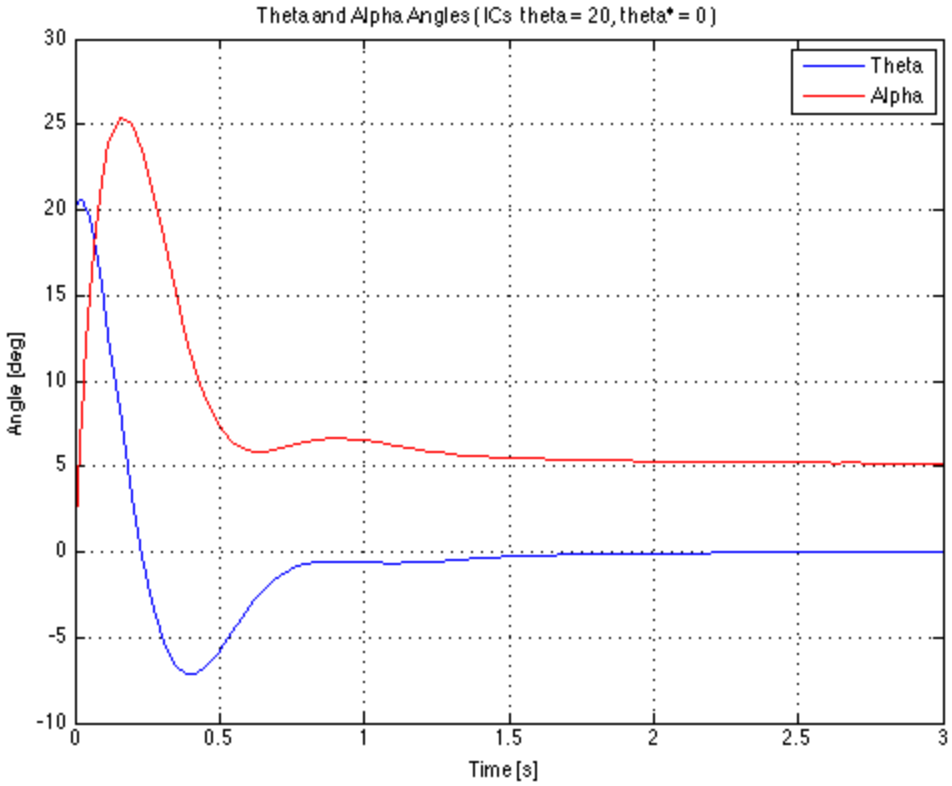
Theta and Alpha Angles (ICs theta = 20, theta* = 0)
Theta
Alpha
Angle [deg]
Time [s]

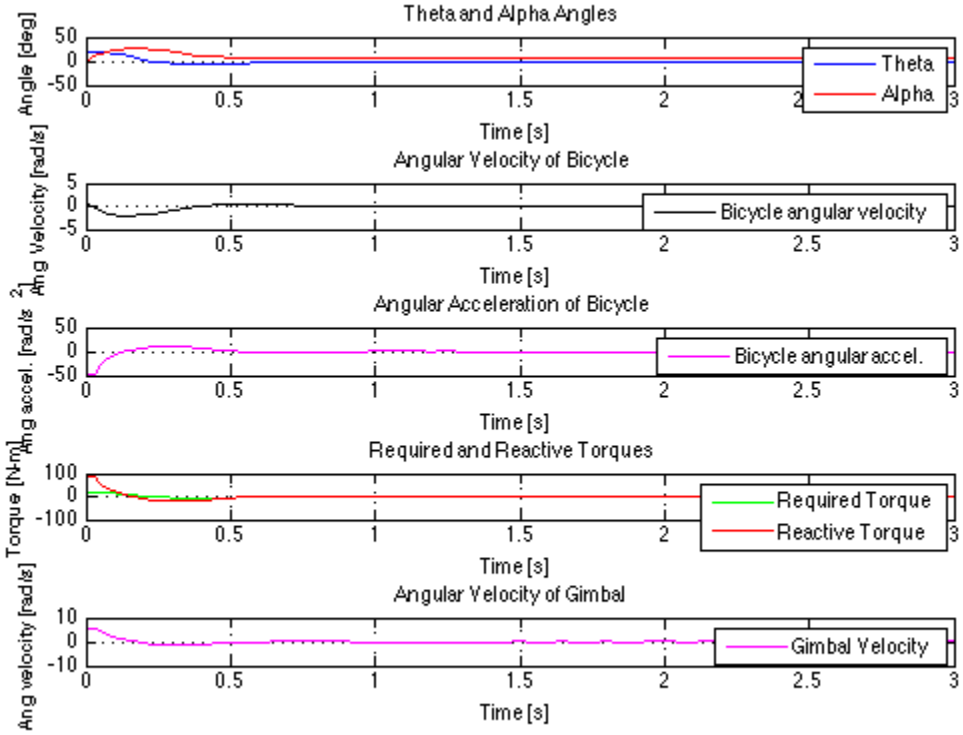
Theta and Alpha Angles
Angle [deg]
Theta
Alpha
Time [s]
Angular Velocity of Bicycle
Ang Velocity [rad/s]
Bicycle angular velocity
Time [s]
Angular Acceleration of Bicycle
Ang accel. [rad/s^2]
Bicycle angular accel.
Time [s]
Required and Reactive Torques
Torque [N-m]
Required Torque
Reactive Torque
Time [s]
Angular Velocity of Gimbal
Ang velocity [rad/s]
Gimbal Velocity
Time [s]

```
clear
close all
clc

%Program generates simulations for the bicycle performing a wheelie


g=9.81;                          %[m/s^2] gravity
den=7850;                        %[kg/m^3] density of steel flywheel (St-7850)(Tur
t=0.032;                         %[m] thickness of flywheel
y_bike=.2465;                    %[m] center of gravity y component
x_bike=.4914;                    %[m] center of gravity x component
w=20000*2*pi()/60;               %[rpm] rev per minute of flywheel
I_bike=8.92;                     %[kg/cm^2] bicycle moment of inertia
r_bike=sqrt(x_bike^2+y_bike^2); %[m] constant distance from bicycles axis of rota
gamma=atan(y_bike/x_bike);


% initial conditions
beta_i=0*pi()/180;             %[rad] initial wheelie angle
beta_d=0;                      %[rad/s] initial angular velocity about z-axis


r_fly=3*.065;                            %[m] radius of flywheel (0.065)
m_fly=pi()*((r_fly).^2)*t*den;          %[kg] mass of flywheel
m_gyro=m_fly*2-(1/3)*m_fly;             %[kg] estimate for the weight of flywheel
                                         % with housing (i.e. weight of whole gyro
m_bike=2*13.14+2*m_gyro;                    %[kg] mass of bike with gyro hardware
L=(0.5)*(m_fly).*(power(r_fly,2)).*w;   %[kg*m^2/s] angular momentum
alphaDmax=5.75;                         %[rad/s] maximum gimbal velocity


Beta_target=35*pi()/180;               %[rad] target theta used as input to contr


sim('sumOfTorqueStabilization2')


beta=beta*180/pi();
alpha=alpha*180/pi();



%************************************************************************
% Individual Plots


plot(time, beta, 'b', time, alpha, 'r')
title(sprintf('Beta and Alpha Angles'))
legend('Beta','Alpha')
xlabel('Time [s]');
ylabel('Angle [deg]')
```

```
grid on


% figure
% plot(time, t_req, 'g', time, t_reactive, 'r')
% title('Required and Reactive Torques')
% legend('Required Torque','Reactive Torque')
% xlabel('Time [s]');
% ylabel('Torque [N-m]')
% grid on
%
% figure
% plot(time, theta_d, 'k')
% title('Angular Velocity of Bicycle')
% legend('angular velocity')
% xlabel('Time [s]');
% ylabel('Ang Velocity [rad/s]')
% grid on
%
% figure
% plot(time, theta_dd, 'm')
% title('Angular Acceleration of Bicycle')
% legend('angular accel.')
% xlabel('Time [s]');
% ylabel('Ang accel. [rad/s^2]')
% grid on
%
% figure
% plot(time, alphaD_prof, 'm')
% title('Angular Velocity of Gimbal')
% legend('Gimbal Velocity')
% xlabel('Time [s]');
% ylabel('Ang velocity [rad/s]')
% grid on




%**********************************************************************
% All Plots on one figure

figure
subplot(5,1,1)
plot(time, beta, 'b', time, alpha, 'r')
title('Beta and Alpha Angles')
legend('Beta','Alpha')
xlabel('Time [s]');
ylabel('Angle [deg]')
grid on

subplot(5,1,2)
plot(time, beta_d, 'k')
title('Angular Velocity of Bicycle')
legend('Bicycle angular velocity')
```

```
xlabel('Time [s]');
ylabel('Ang Velocity [rad/s]')
grid on

subplot(5,1,3)
plot(time, beta_dd, 'm')
title('Angular Acceleration of Bicycle')
legend('Bicycle angular accel.')
xlabel('Time [s]');
ylabel('Ang accel. [rad/s^2]')
grid on

%figure
subplot(5,1,4)
plot(time, t_req, 'g', time, t_reactive, 'r')
title('Required and Reactive Torques')
legend('Required Torque','Reactive Torque')
xlabel('Time [s]');
ylabel('Torque [N-m]')
grid on


subplot(5,1,5)
plot(time, alphaD_prof, 'm')
title('Angular Velocity of Gimbal')
legend('Gimbal Velocity')
xlabel('Time [s]');
ylabel('Ang velocity [rad/s]')
grid on
```

Warning: Using a default value of 0.08 for maximum step size. The simula
step size will be equal to or less than this value. You can disable this
diagnostic by setting 'Automatic solver parameter selection' diagnostic t
'none' in the Diagnostics page of the configuration parameters dialog

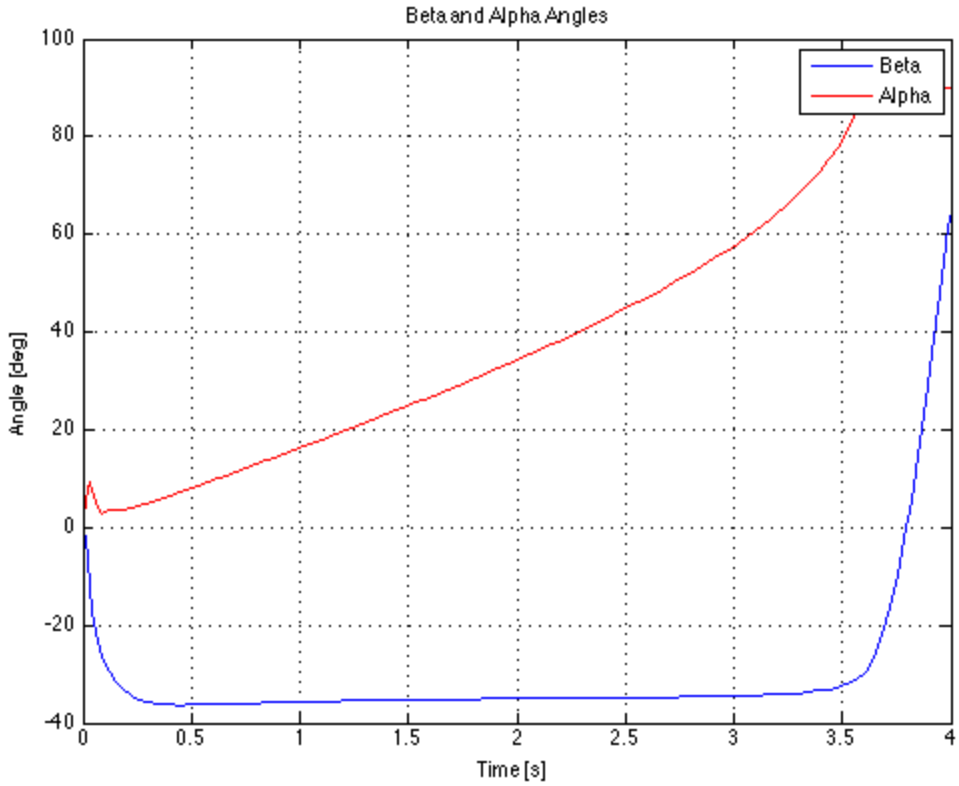
Beta and Alpha Angles
Beta
Alpha
Angle [deg]
Time [s]

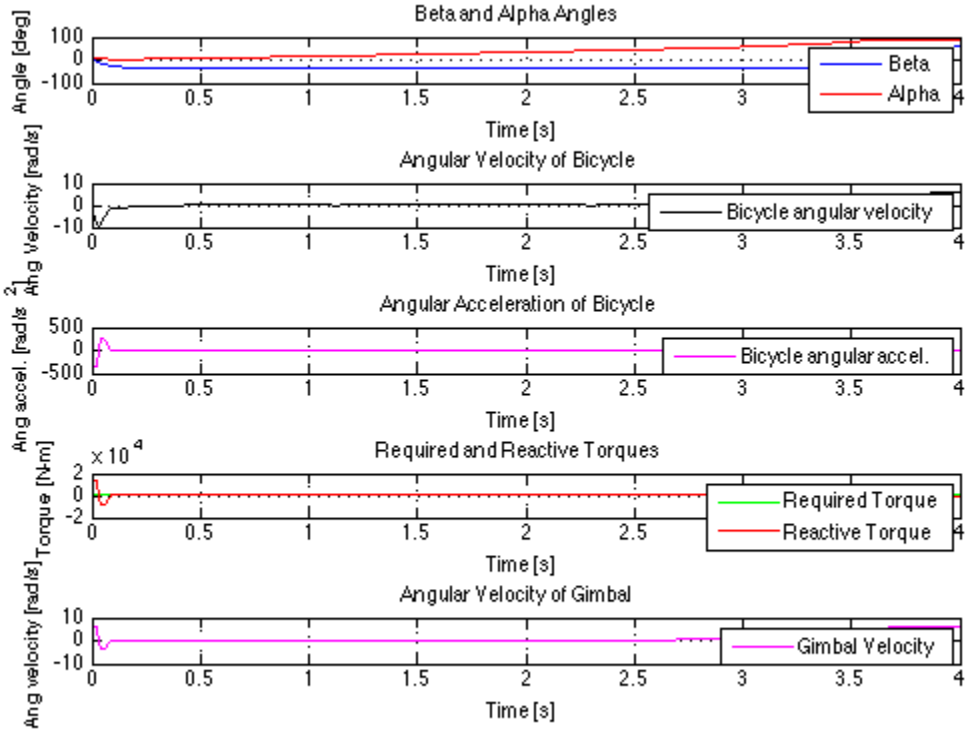
Beta and Alpha Angles
Angle [deg]
Beta
Alpha
Time [s]
Angular Velocity of Bicycle
Ang Velocity [rad/s]
Bicycle angular velocity
Time [s]
Angular Acceleration of Bicycle
Ang accel. [rad/s^2]
Bicycle angular accel.
Time [s]
Required and Reactive Torques
x 10^-4
Torque [N-m]
Required Torque
Reactive Torque
Time [s]
Angular Velocity of Gimbal
Ang velocity [rad/s]
Gimbal Velocity
Time [s]